



## Annual Dynamics of Global Land Cover and its Long-term Changes from 1982 to 2015

Han Liu<sup>1</sup>, Peng Gong<sup>1,2</sup>, Jie Wang<sup>2,3</sup>, Nicholas Clinton<sup>4</sup>, Yuqi Bai<sup>1</sup>, Shunlin Liang<sup>5,6</sup>

<sup>1</sup>Ministry of Education Key Laboratory for Earth System Modeling, Department of Earth System Science, Tsinghua University,

5 Beijing, 100084, China

<sup>2</sup>AI for Earth Lab, Cross-Straits Institute, Tsinghua University, Beijing, 100084, China

<sup>3</sup>State Key Laboratory of Remote Sensing Science, Institute of Remote Sensing and Digital Earth, Chinese Academy of Sciences, Beijing, 100101, China

<sup>4</sup>Google LLC, 1600 Amphitheatre Parkway, Mountain View, CA 94043 USA

10 <sup>5</sup>Department of Geographical Sciences, University of Maryland, College Park, MD 20742 USA

<sup>6</sup>School of Remote Sensing Information Engineering, Wuhan University, Wuhan, 430072, China

*Correspondence to:* Peng Gong ([penggong@tsinghua.edu.cn](mailto:penggong@tsinghua.edu.cn)), Jie Wang ([sohuwangjie@163.com](mailto:sohuwangjie@163.com))

**Abstract.** Land cover (LC) is an important terrestrial variable and key information for understanding the interaction between human activities and global change. As the cause and result of global environmental change, land cover change (LCC)

15 influences the global energy balance and biogeochemical cycles. Continuous and dynamic monitoring of global LC is urgently needed. Effective monitoring and comprehensive analysis of LCC at the global scale is rare. Using the latest version of GLASS (The Global Land Surface Satellite) CDRs (Climate Data Records) from 1982 to 2015, we built the first set of CDRs to record the annual dynamics of global land cover (GLASS-GLC) at 5 km resolution using the Google Earth Engine (GEE) platform. Compared to earlier global LC products, GLASS-GLC is characterized by high consistency, more detailed classes, and longer 20 temporal coverage. The average overall accuracy is 85 %. We implemented a systematic uncertainty analysis at the global scale. In addition, we carried out a comprehensive spatiotemporal pattern analysis. Significant changes and patterns at various scales were found, including deforestation and agricultural land expansion in the tropics, afforestation and forest expansion in northern high latitudes, land degradation in Asian grassland and reclamation in northeast China, etc. A global quantitative analysis of human factors showed that the average human impact level in areas with significant LCC was about 25.49 %. The 25 anthropogenic influence has a strong correlation with the noticeable Earth greening. Based on GLASS-GLC, we can conduct long-term LCC analysis, improve our understanding of global environmental change, and mitigate its negative impact.

GLASS-GLC will be further applied in Earth system modeling in order to facilitate research on global carbon and water cycling, vegetation dynamics and climate change. The data set presented in this article is published in the Tagged Image File Format (TIFF) at <https://doi.org/10.1594/PANGAEA.898096>. The data set includes 34 TIFF files and one instruction doc file.



30 **1 Introduction**

Land cover (LC) is the physical evidence on Earth. It is the result of both natural and human forces (Running, 2008; Sterling et al., 2013; Tucker et al., 1985; Gong et al., 2013; Yang et al., 2013). It is an important source of information to understand the complex interaction between human activities and global changes (Lambin et al., 2006). LC data is one of the most important variables needed to bring about the nine large social benefits in the field of Global Earth Observation Systems (Herold et al., 35 2008). Land cover change (LCC) is the cause and result of global environmental change (Turner et al., 2007), and it can change the energy balance and biogeochemical cycles (DeFries et al., 1999; Claussen et al., 2001), further affecting climate change and surface attributes and the provision of ecosystem services (Pielke, 2005; Zhao et al., 2001; Gibbard et al., 2005; Reyers et al., 2009). Therefore, a long time series of LCC information is critical to the understanding of global environmental change (Matthews et al., 2004). LC and LCC information is also valuable to resource management, biodiversity conservation, food 40 security, forest carbon, etc (Houghton et al., 2012; Achard et al., 2004; Andrew K et al., 2015). Therefore, more frequent land cover information at the global scale is highly desirable.

However, LC is highly dynamic due to changes in natural phenology and human activities (Lambin et al., 2001). This characteristic poses a huge challenge to mapping and monitoring (Verburg et al., 2009; Lepers et al., 2005; Rindfuss et al., 2004), and an effective quantitative analysis of global LCC is lacking (Ramankutty et al., 2006). The traditional method of LC 45 mapping based on field studies can hardly be applied to large areas due to the required amount of labor (Gong, 2012). In addition, any mapping results obtained in this way would be difficult to update in a timely manner. Satellite observations are the most economical and feasible means of large-scale LC monitoring (Fuller et al., 2003; Rogan and Chen, 2004). Due to the development of satellite sensors, the continuous accumulation of historical satellite data, and the advancement of relevant image processing algorithms, LC monitoring can be effectively carried out (Cihlar, 2000; Pal, 2005; Gallego, 2004; Chen et al., 50 2018). However, previous monitoring mainly focuses on the mapping of a particular area (Liu et al., 2002; Brink and Eva, 2009; Yuan et al., 2005; Margono et al., 2012; Feng et al., 2018) or in a single period (Homer et al., 2004), and because of the differences in data sources and mapping methods, the consistency of mapping results between different sources and periods is poor and lacks comparability, making it difficult to quantify the changes effectively (Friedl et al., 2010).

Automatic mapping methods depend highly on the sample dataset for its representativeness, quantity and quality due to the 55 considerable heterogeneity at the global level (Gong et al., 2013; Li et al., 2014). A combination of a comprehensive global sample dataset, professional interpretation and support from mapping teams are needed (Li et al., 2017). In general, sample LC data are mainly collected from field visits or manual interpretation (Li et al., 2016; Hansen et al., 2000). Generalization from higher resolution LC map products can also be useful for coarser resolution mapping purposes (Song et al., 2018a). The former is more accurate and effective, but requires much manpower, resource and effort (Li et al., 2016); the latter is a feasible 60 option and is more efficient but largely depending on the accuracy of the parent product.



A number of global LC products exists. Some examples include the 30 m Finer resolution observation and monitoring of global land cover (FROM-GLC) (Gong et al., 2013), the 1992-2015 annual 300 m global land cover data (<http://maps.elie.ucl.ac.be/CCI/viewer/index.php>), MODIS global land cover product (Friedl et al., 2010), 1 km International Geosphere-Biosphere Programme Data and Information System Cover map (IGBP-DISCover) (Loveland et al., 2000), 1 km

65 University of Maryland (UMD) land-cover map (Hansen et al., 2000), 1 km Global Land Cover 2000 (GLC2000) map (Bartholome and Belward, 2005). These mapping results tend to focus on a single or short period of time, and because of their different classification systems and resolutions, they are difficult to compare (Ban et al., 2015;Grekousis et al., 2015). However, high-resolution mapping results can be used as an effective reference for low-resolution mapping (Song et al., 2018a;DeFries et al., 1998). Therefore, when performing lower-resolution global mapping, it is possible to consider directly generating

70 training samples from high-resolution global mapping results, which will meet the mapping requirements, (Wang et al., 2016). Long time-series LC mapping requires high consistency of data sources, and also has certain requirements for multi-period samples (Wardlow and Egbert, 2008). The commonly used satellite data that cover a long period of time (more than 30 years) include the Advanced Very High Resolution Radiometer (AVHRR) data and Landsat imagery (Giri et al., 2013;Franch et al., 2017;Wulder et al., 2008). While Landsat data has higher resolution, in many areas they are more prone to cloud, consistency

75 and data volume (Gómez et al., 2016;Wulder et al., 2008;Xie et al., 2018). AVHRR data has a low spatial resolution, and the quality of the raw AVHRR data is poor. The requirements for pre-processing and consistency processing such as cloud removal and missing value filling are high. The GLASS CDRs based on AVHRR data tend to have better data consistency due to the systematic data production (Liang et al., 2013). Using such data for LC mapping can significantly improve the consistency and comparability of mapping results, and thus can be effective in supporting change analysis. If the consistency of the original 80 data source used is not good enough, it may be necessary to collect annual samples for classification to ensure the reliability of change analysis (Xu et al., 2018).

Recently, some attempts have been made to map global LC over a long time series, but these have focused on a single class (such as water bodies (Wood et al., 2011;Pekel et al., 2016), impervious surface (Schneider et al., 2010;Zhang and Seto, 2011), cropland (Pittman et al., 2010), etc.) or a few classes (such as Vegetation Continuous Fields (VCF) (Song et al., 2018a), mainly 85 depicting vegetation changes). General purpose multi-class land cover mapping over a period of over 30 years does not exist before.

Because of the lack of long time-series general purpose global LC maps, using the Google Earth Engine (GEE) platform (Gorelick et al., 2017), we produced the first CDR set of consistent and reliable LC products, GLASS-GLC, covering the period from 1982 to 2015. The data used was primarily the 0.05 ° AVHRR-based GLASS CDRs. The classification system is 90 adjusted from the FROM-GLC according to the data characteristics. Below, we describe the methods used, results obtained with some preliminary change analysis.



## 2 Data and methods

The framework for mapping GLASS-GLC is shown in Fig. 1. It includes annual feature collection and construction, training sample generation, classification and time consistency adjustment, accuracy assessment and product inter-comparison. The 95 entire framework is implemented in the GEE. The GEE is a cloud-based platform for planetary-scale geospatial analysis that brings Google's massive computational capabilities to bear on a variety of high-impact societal issues including deforestation, drought, disaster, disease, food security, water management, climate monitoring and environmental protection (Gorelick et al., 2017). We uploaded GLASS data to GEE and did subsequent analysis in GEE.

### 2.1 Data

100 The annual feature collection from 1982 to 2015 involves a variety of data products, the most important of which is the latest version of GLASS CDRs. CDRs require data with a long time series, high consistency and high continuity, which is not the same as the commonly-used remote sensing products (Hollmann et al., 2013; Cao et al., 2008). Derived from AVHRR data, the GLASS CDRs include a wide range of surface parameters that are important for LC classification (<http://glass-product.bnu.edu.cn/>). The products have a spatial resolution of 0.05 °, a temporal frequency of 8 days with a time span of 105 1982-2015. In our study, Normalized Difference Vegetation Index (NDVI), Leaf Area Index (LAI) (Xiao et al., 2016), Fraction of Absorbed Photosynthetically Active Radiation (FAPAR) (Xiao et al., 2015), Evapotranspiration (ET) (Yao et al., 2014), Gross Primary Production (GPP) (Yuan et al., 2010), Broadband Emissivity (BBE) (Cheng et al., 2016), White-sky Albedo in Visible band (ABD\_WSA\_VIS), White-sky Albedo in Near Infrared band (ABD\_BSA\_NIR) and White-sky Albedo in Shortwave band (ABD\_WSA\_shortwave) (Qu et al., 2014) are the variables used for subsequent classification.

110 To provide further reference, vegetation cover fraction (VCF) products are used to aid classification. The VCF products express the surface as a combination of vegetation proportions according to information from remotely sensed data. To match the resolution of the GLASS CDRs, the VCF products used here (Song et al., 2018a) also have a spatial resolution of 0.05 °, and are obtained from the Land Processes Distributed Active Archive Center (<https://lpdaac.usgs.gov/>). These products are mainly based on AVHRR, and the interannual consistency has been maintained. Based on the training samples from Landsat products 115 from around 2000 (Hansen et al., 2013; Ying et al., 2017), with a supervised regression tree model, the VCF products from 1982 to 2016 (data missing in 1994 and 2000) were generated, and were composed of the percentages of tree canopy (TC), short vegetation (SV) and bare ground (BG) in each pixel.

In addition, in order to enhance the distinguishing capacity, we also used terrain data provided by the Global Multi-resolution Terrain Elevation Data of 2010 (GMTED2010). Based on the elevation data, the slope information can be further calculated 120 to reflect the terrain and help to distinguish different vegetation types growing on steep slopes to those on level ground. The dataset comes from the GEE platform and contains 2010 Earth Elevation data collected from various sources. The primary source is the Shuttle Radar Topography Mission (SRTM) Digital Terrain Elevation Data (DTED) (void-filled) 1-arc-second



data. Other sources are used for filling the gaps in areas outside the SRTM coverage. As the terrain is relatively stable over years, using the data of one single year is plausible. The spatial resolution of the GMTED2010 data used is 7.5 arc seconds and it has been upsampled to 5 km in subsequent analyses.

## 2.2 Classification system

The classification system in FROM-GLC Version 2 (FROM-GLC\_v2) defines eleven Level 1 classes that can be easily mapped to the Food and Agricultural Organization of the United Nations (FAO) LC Classification System and the International Geosphere–Biosphere Programme (IGBP) classification system (Wang et al., 2015). This classification system evolved from the classification system of FROM-GLC Version 1 (Gong et al., 2013) with addition of leaf information.

We adjusted some classes of the original classification system according to the spatial resolution and situation of the used data. Because the data used here are land surface products, where the water surface has been masked, the class of "water bodies" cannot be extracted from the GLASS dataset. Wetland is a highly variable class and impervious surface whose patches are small in size. They are difficult to identify at the spatial resolution of 0.05 °(Wang et al., 2015). Thus, the water body, impervious surface, and wetland classes were not included in this work, and they shall be derived with more specialized methods. While water and impervious surface mapping have achieved satisfactory results (Ji et al.;Gong et al., submitted), wetland mapping remains a great challenge (Gong et al., 2013). In addition, the "cloud" class was removed. The adjusted classification system consists of 7 classes, including cropland, forest, grassland, shrubland, tundra, barren land, snow/ice, as shown in Table 1.

## 140 2.3 Training samples

In order to obtain the training samples, we adopted the majority-class synthesis strategy. First, we projected the 30m FROM-GLC\_v2 results, that were created using Landsat data acquired mainly from 2013-2015 (Li et al., 2017), into a 0.05 ° coordinate system. By calculating the area ratio of each class in each 0.05 ° pixel, the class with the greatest area ratio in each pixel was used as the new class label in the aggregated 0.05 ° mapping results. Subsequently, sample points were randomly generated (with a limited interval greater than 0.1 °) with the class label obtained from the aggregated FROM-GLC\_v2 0.05 ° mapping result (adjusted to be consistent with the new classification system). Finally, 10,000 training sample units were obtained. The spatial distribution of training sample units is shown in Fig. 2, and the class distribution of training samples is shown in the inner pie chart.

## 2.4 Feature collection

150 We constructed a feature collection with a strong discrimination ability to detect LC from multiple aspects such as terrain, phenology, spectrum, and spectral index, etc. The annual percentiles (including 0, 10, 25, 50, 75, 90, 100) of all bands of the



GLASS CDRs and the mean and standard deviation of the NDVI between two adjacent percentiles are calculated, as an annual feature collection from GLASS CDRs. Among them, the percentile that represents specific phenological information can provide simplified time series information, reduce the noise of annual time series, and help improve the classification accuracy

155 (Hansen et al., 2013). By extracting the statistical information between adjacent percentiles, the time series information can be further supplemented. Due to the systematic deviation of AVHRR products (Song et al., 2018b), in order to ensure the inter-annual consistency of the GLASS features, we used the processing method developed for generating the VCF products, with the corresponding MODIS products for end-member correction, where desert and intact forest are regarded as the end-element of each pixel (Song et al., 2018a). After the correction, the inter-annual inconsistency of feature collection from the GLASS  
160 CDRs is improved. Figure 3 shows the time series of the global median value of the GLASS ABD\_WSA\_VIS band, where the orange one represents the curve before the correction and the grey one is the result after the correction. It can be seen that after the correction, the fluctuations of the feature become smaller, and the individual abnormal values are also adjusted.

Taking into account the time span of the GLASS CDR-based feature collection, the VCF products from 1982 to 2015 are used, with the missing 1994 and 2000 data supplemented by calculating the average of the adjacent years. There are three features  
165 of the percentage of tree cover (TC), short vegetation (SV) and bare ground (BG) for each year. Based on the GMTED2010 dataset, the slope information is calculated and finally added to obtain an average slope value for each 0.05 ° pixel. In addition, the central latitude and longitude information of each 0.05 ° pixel is also recorded as part of the input features. Finally, an annual collection of 81 input features for the period of 1982 to 2015 was constructed, including the annual GLASS CDR percentile feature (7×9), the mean and standard deviation of the NDVI annual adjacent percentiles (6×2) and VCF features (3),  
170 assisting the slope information (1) and latitude (1), longitude (1) information (Table 2).

## 2.5 Classification and time consistency

We used a random forest classifier for global LC mapping following the good performance of the random forest classifier in the machine learning field (Rodriguez-Galiano et al., 2012;Pal, 2005). The number of trees was 200, and other parameters were set as default. The classifier was trained using the training sample with an annual feature collection constructed as the  
175 input. The global LC maps from 1982 to 2015 were obtained using the trained classifier.

In order to further ensure the time consistency of the mapping results, we used the “LandTrendr” method (Kennedy et al., 2010;Cohen et al., 2018) and implemented a linear regression-based algorithm for the constructed annual feature collection to find the breakpoints in the time series (Li et al., 2018). The class labels in the time series between adjacent breakpoints will be updated to the mode of the class label time series for the time period. Through this strategy, we can smooth the time series of  
180 the mapping results, avoid noise interference as much as possible, and finally get the adjusted GLASS-GLC.



## 2.6 Accuracy assessment

To verify the reliability of GLASS-GLC CDR products from multiple perspectives, we performed accuracy assessments and uncertainty analyses. Testing samples was extracted from the 30m resolution FROM-GLC\_v2 (Li et al., 2017) to evaluate the 2015 LC mapping results. First, we dropped those sample units whose classes were not included in our classification system.

185 The remaining test samples units were then overlapped with the abovementioned aggregated 0.05 ° FROM-GLC\_v2 mapping result, and only those whose class labels were consistent were kept. These were regarded as huge homogeneous samples (H-homo samples) reserved as the final test samples. A total of 23459 huge homogeneous test samples units from FROM-GLC\_v2 were obtained to test the 2015 global LC mapping result. In addition, another 525 test samples units from the FLUXNET site data (Gong, 2009) for 2015 were selected to supplement the test samples to further test the 2015 result. The distribution of the 190 entire test samples in 2015 is shown in Fig. 4, where the class distribution of the test samples is shown in the inner pie chart. In addition to obtaining the classification confusion matrix in 2015 based on the above test samples, in order to identify regions where classification is difficult, an uncertainty analysis was carried out. The incorrect test samples locations are marked as 1, while the correct test samples locations are marked as 0. The spatial distribution map of the uncertainty of the LC mapping result in 2015 is depicted based on a Kriging interpolation method (Oliver and Webster, 1990). The search radius parameter of 195 Kriging interpolation is set to 12 nearby points, the other parameters as default. The value of the uncertainty ranges from 0 to 1. A value near 0, indicates a lower uncertainty while a value near to 1, indicates a higher uncertainty and a higher possibility of misclassification.

## 2.7 Statistical analysis

To extract the area of LCC, we estimated the trend of change through statistical analysis and avoided the influence of abnormal fluctuations from the obtained long time series of global LC products. The annual area of each class on the scales of latitudinal zones, continents are summarized. A time series of the annual area for each class was generated. The boundary data of countries and continents were obtained from the Bureau of Surveying and Mapping of China. Eco-region data were obtained from the FAO global eco-region dataset (Simons et al., 2001) (<http://www.fao.org/geonetwork/srv/en/metadata.show?CurrTab=simple&id=1255>).

205 Although the inter-annual consistency has been ensured as much as possible in the above mapping framework, the effects of inter-annual changes due to climate conditions and phenological changes were removed by fitting a linear trend (Theil-Sen estimator (Sen, 1968)) to estimate the long-term trend of change in area for each class, where the annual change slope and the 95 % confidence interval of the slope is given. In addition, a Mann-Kendall test (Mann, 1945) was used to test the trend of time series and the p-value is given. If  $p < 0.05$ , it is considered that the trend of change is significant.  
210 Further, we got the change mask where all pixels showed a significant change trend guaranteed by statistical hypothesis testing (Wang et al., 2016). First, we downscaled the grid from 0.05 ° to 0.25 °, and the time series of the area ratio of all classes in



each  $0.25^{\circ}$  grid was summed. Using the Mann-Kendall test, those grids showing a significant change ( $p < 0.05$ ) were obtained.

Then the annual change in slope of area ratio for each grid with an increasing or decreasing trend was found using a Theil-Sen estimator. The change ratios were then summarized for the regional scales to estimate the corresponding significant areas of

215 change from 1982 to 2015.

### 2.8 LC conversion

In order to quantify the magnitude of global LCC between 1982 and 2015 and reveal the global temporal LCC pattern, we calculated the ratio of annual global LCC to the global total terrestrial LC area by different time periods. To ensure the quantified LCC to be non-accidental, we limited the computation area within the change mask in which all grids show a 220 statistically significant loss or gain trend. We then summarized the annual LCC by 5-year and 10-year time intervals, respectively.

To further identify the direct causes of LCC, we assessed the LC conversion from 1982 to 2015. Based on the  $0.05^{\circ}$  LC mapping results of 1982 and 2015, a map of LC conversion can be obtained. The computation was also limited to the change mask to ensure the statistical significance. The conversion sources and destinations of LC classes were separately computed,

225 so as to directly assess the direct causes of change in various classes of LC.

### 2.9 Human impact

To further explore the role of human impact in regions with significant LCC, the results are evaluated based on data from the human impact campaign (Fritz et al., 2017), which can be downloaded from

<https://doi.pangaea.de/10.1594/PANGAEA.869680>. The original study area was generated in the 2011 campaign to evaluate a 230 map of land availability for biofuel production (Fritz et al., 2013), collected using a Geo-Wiki crowdsourcing platform. Pixels with a resolution of 1 km were randomly provided to volunteers. For each pixel, volunteers needed to point out the overall degree of human impact (HI, 0–100 %) which was visible from Google Earth's high-resolution satellite image and they were required to provide confidence levels in four categories: unsure; less sure; quite sure; and sure. Here, HI refers to the degree to which the landscape modified by humans visible from satellite images (Fritz et al., 2017). A total of 151942 point-records

235 are available. To get the global distribution map of HI, we performed Kriging interpolation on the point records that had previously excluded the category of unsure confidence level. The search radius parameter of the Kriging interpolation was set to 12 nearby points and the other parameters as default. As shown in Fig. 5, we can see that the interpolation results reflect the global distribution of the intensity of human activity.



### 3 Results

#### 240 3.1 Reliability of the products

The global LC mapping result in 2015 is shown in Fig. 6. Its accuracy was tested with the H-homo sample in 2015 to obtain a confusion matrix (Table 3). The overall accuracy for the year 2015 reached 86.51 %. As for each class, the accuracies of forest, barren land and tundra are relatively high, where the user's accuracies and producer's accuracies are over 90 %. The accuracy of cropland is also high, with the user's accuracy and producer's accuracy reaching 73.54 % and 78.62 %, respectively. The user's accuracy of shrubland reached 83.62 %, while that of grassland is 67.58 %. Grassland is mainly mixed with cropland and shrubland. Table 4 shows the testing results of the FLUXNET test samples in which the number of sample units for shrubland, tundra, barren land, and snow/ice are relatively small. The overall accuracy of all classes is 82 % tested against the FLUXNET sample. Among them, the user's accuracy and the producer's accuracy for forest reach 91 % and 88 %, respectively. The producer's accuracy for cropland is 69 %, while its user's accuracy is 73 %.

250 Putting the test results from FROM-GLC\_v2 and FLUXNET together, a spatial distribution map of the uncertainty of the 2015 LC mapping result was generated. As can be seen from Fig. 7, most of the world is shown in a green color, which means that the mapping result for most regions is most likely to be correct, and the result for 2015 is highly credible. There are still some regions showing a yellow or orange color, and a smaller number of regions showing red, representing those regions that may have been misclassified. Since there are no test samples in Greenland, the interpolation results are ignored. In general, the 255 places with high uncertainty are Africa, East and South America, South Alaska, North and East Australia and Southwest Indonesia.

#### 3.2 Spatiotemporal patterns in LCC

##### 3.2.1 Global temporal patterns

Figure 8 shows the variation curves of the global area for various LC classes from 1982 to 2015, where dotted lines are the corresponding trend lines. Overall, the global area of forest increases significantly ( $p = 0.0000$ ) from 1982 to 2015. As for shrubland, although fluctuating, it shows a significant increasing trend ( $p = 0.0017$ ). The global area of grassland, tundra, barren land snow/ice significantly decreases with  $p = 0.0000$ ,  $p = 0.0019$ ,  $p = 0.0000$ , and  $p = 0.0003$  respectively.

Figure 9 shows the ratio of annual global LCC to the global total terrestrial LC area, calculated by different time periods, where Fig. 9(a) shows the results with a 5-year interval and Fig. 9(b) with a 10-year interval. Overall, the annual ratio ranges from 265 0.35 % to 0.70 %, with an average of 0.52 % between 1982 and 2015. 5-year interval ratios show a relatively fluctuating trend. The average ratio reaches 0.63 % in 1991-1995, the highest among the seven intervals. The ratios have relatively large fluctuations in 2006-2010. All in all, the ratios before 1995 are generally higher, and it gradually decreases since then. With 10-year interval, ratios after 2000 are generally lower with an average of only 0.40 % in 2011-2015.



### 3.2.2 Patterns along latitudinal gradients

270 The global distribution of 0.25 ° grids with significant LCC from 1982 to 2015 is shown in Fig. 10 for the whole world, where the color depth represents the estimated change in area ratio per year. The distribution of significant LCC along latitudes is shown in the right, where the red curve represents a significant increase, green a significant decrease, and blue a net change. The distribution pattern of LCC along latitudes is different, especially for cropland and forest, where it can be seen that cropland has increased significantly in the northern tropics and the southern hemisphere. It is confirmed that the significant increase in 275 cropland has occurred mainly in the tropics and southern hemisphere (Gibbs et al., 2010). Forest has decreased significantly in the southern hemisphere and has increased significantly in the northern hemisphere, showing regional differences. In particular, in the high latitudes of the north, forest has increased significantly with a decrease of tundra. However, the increase in forest area in the northern hemisphere is significantly larger than that in the southern hemisphere, reflecting an overall increase in total forest area.

280 The grassland area has reduced at almost all latitudes. This phenomenon may reflect the degradation of grassland. On the other hand, there might exist an increased trend in global vegetation coverage, where shrubland and forest expansion led to a reduction in the grassland area. It can be seen that shrubland has increased significantly in the southern hemisphere, corresponding to the reduction in the grassland area there. The area of barren land is decreasing, especially in the middle and high latitudes of the north, which further reflects the increase in vegetation coverage. The area of snow/ice in the northern high 285 latitudes has reduced.

### 3.2.3 Continental patterns

The statistical results for each class at the continental scale are shown in Table 5, Table 6, Table 7, Table 8, Table 9, Table 10 and Table 11, where the slope and p-values are estimated according to the class area time series, while gain and loss are the computed values from 0.25 ° grids with significant LCC.

290 There is significant geographical heterogeneity among continents due to differences in latitude and longitude, as well as economic and social development differences, where significant causes of LCC are from both natural and human influences (Lambin et al., 2001).

Cropland significantly increased in South America, with a growth rate of  $9.1 \times 10^3 \text{ km}^2/\text{year}$  ( $p = 0.0108$ ). The area of significantly increased cropland in Asia and Africa reached  $67 \times 10^3 \text{ km}^2$  and  $23 \times 10^3 \text{ km}^2$ , respectively. Many developing

295 countries in South America, Asia and Africa have relatively poor economic and social development, rapid population growth and increasing demand for food (Barbier, 2004). At the same time, the international demand for food has increased, stimulating the export of crop products and requiring access to new land, which ultimately leads to the expansion of cropland.

Corresponding to the increase in cropland, forest decreased significantly in South America, at a rate of  $10.8 \times 10^3 \text{ km}^2/\text{year}$  ( $p = 0.0242$ ). Meanwhile, the area of forest in Africa has significantly decreased by  $29 \times 10^3 \text{ km}^2$ . In addition to cropland



300 expansion, the production of fuelwood and charcoal is also an important driving factor for deforestation (Hosonuma et al., 2012).

The area of forest in Asia has increased at the fastest speed. The area of forest in Europe and North America has also increased significantly. Meanwhile, the tundra area in Asia, Europe and North America decreased significantly by  $132 \times 10^3 \text{ km}^2$ ,  $12 \times 10^3 \text{ km}^2$  and  $22 \times 10^3 \text{ km}^2$ , respectively. The increase of forest in Asia, Europe and North America is related to afforestation projects 305 and forest restoration policies in some regions (Aide et al., 2013; Pan et al., 2011). On the other hand, the increase of forest and the decrease of tundra in the northern high latitudes may be the result of climate warming which promotes forest growth (Zhu et al., 2016). Many studies have shown that in the past 30 years, a warming climate with rising temperatures and melting ice and snow has promoted vegetation growth i.e. greening in the north (Myneni et al., 1997; Park et al., 2016).

Shrubland has increased significantly in Africa at a rate of  $47.4 \times 10^3 \text{ km}^2/\text{year}$  ( $p = 0.0030$ ). Shrubland also increased 310 significantly in Oceania, by an area of  $38 \times 10^3 \text{ km}^2$ . The main source of shrubland conversion is grassland, which can be regarded as another manifestation of greening, where a warming climate makes vegetation grow more vigorously and plant height increase.

The degradation of grassland in Asia is serious. The area of grassland in Asia decreased significantly by  $315 \times 10^3 \text{ km}^2$ , which 315 may be due to drought (Dangal et al., 2016; Zhang et al., 2018). At the same time, human activity may also play a significant role. Another reason is overgrazing that may lead to grassland degradation, and the development of irrigation agriculture that can seriously reduce groundwater levels, which will further aggravate drought (Dubovik et al.). Barren land in Asia also significantly decreased by  $82 \times 10^3 \text{ km}^2$ , which may imply the effects of desertification control in some regions. The global snow/ice area has decreased significantly, at a speed of  $19.2 \times 10^3 \text{ km}^2/\text{year}$  ( $p = 0.0003$ ), reflecting the melting of ice and snow under a warming environment.

### 320 3.3 Characteristics of LC coversion

Whether LCC is caused by natural or human factors, there is often a significant coupling effect. We attempted to find out some high-frequency LC class conversions for the period 1982 to 2015 (Table 12). In addition, the conversion sources and destinations of each LC class are computed separately, as shown in Fig. 11.

Among land converted to cropland in 2015, grassland was the biggest source, accounting for 67.58 %, which indicated that a 325 large amount of cropland came from reclamation (Liu et al., 2005). 6.61 % of cropland was converted from forest, showing the process of forest destruction. Among land converted to forest, the proportion of cropland reached 21.74 %, partly due to the fact that abandoned croplands were restored to forest. Barren land and grassland were respectively the large sources of grassland and barren land, reflecting the dynamic transformation between the two classes. Grassland accounted for 35.00 % of the increasing source of barren land, indicating the process of land degradation (Bai et al., 2008).

330 The most frequent direction of conversion from cropland in 1982 was forest, which reached 78.22 %, reflecting the process of



forest expansion. At the same time, forest was also the main cause of loss of grassland and shrubland, which also confirms the process of forest expansion. The conversion of forest to grassland accounted for 59.04 % of all conversions from forest. The main conversion direction of tundra was forest, reaching 64.60 %, indicating an expansion of forest in the high latitudes of the northern hemisphere.

335 Overall, the increase of forest accounted for the highest proportion of all conversion processes, reaching 44.17 %, reflecting the phenomenon of forest expansion. The increase of grassland and cropland were second and third highest, reaching 19.79 % and 13.64 %, respectively, showing the phenomenon of cropland and pasture expansion. In addition, the proportions of grassland to shrubland and barren land to grassland were 7.73 % and 5.75 %, respectively. Cropland expansion and surface greening were the main phenomena reflected by the changes in global LC from 1982 to 2015.

### 340 3.4 Human impact

Figure 12 shows different human impact (HI) levels among different LCC areas. Overall, the average HI level in regions with significant changes in all LC classes is 25.49 %, indicating that human activity has a great impact on LCC (Meyer and Turner, 1992). The highest HI level was found in those regions with significant increases in cropland, reaching an average value of 51.38 %. Meanwhile, the HI level of cropland loss reached 48.02 % while the HI level for forest loss was 26.91 %. In addition, 345 in any change of natural vegetation, such as forest, grassland and shrubland, the HI level in regions of vegetation loss is higher than that of gain, which indicates that human activity has a destructive effect on natural vegetation, while other factors may promote an increase in natural vegetation (Richardson et al., 2013; Cramer et al., 2001).

The HI levels along continents can be found in Fig. 13. The highest level of HI is found in Europe and lowest in Oceania. The HI in Europe reached 46.86 %, indicating that human activity played a relatively important role in regions with significant 350 LCC. Asia came second, with an HI level of 32.07 %. In South America and Oceania in the southern hemisphere, the overall HI level in the LCC regions is small.

As shown in Fig. 14, the polar regions and the boreal coniferous forest regions at northern high latitudes with significant LCC have lower HI levels, indicating that LCC in those regions may be more related to natural factors like climate change (Buermann et al., 2014; Macias-Fauria et al., 2012). The level of HI in subtropical regions is high, among which HI levels in 355 subtropical steppe and subtropical humid forest regions reached 38.23 % and 43.90 %, indicating that the role of LC conversion caused by human activity in subtropical climate areas is significant. In addition, in the temperate steppe regions, the HI level in the regions of significant LCC is also high, reaching 39.87 %, which may be due to intense grazing from agricultural activities (Marlon et al., 2008; Bellwood et al., 2011), resulting in the higher HI level. In the tropics the average HI level in dry forest regions is highest among regions of significant LCC, reaching 34.04 %. Such HI level in this eco-region may be caused 360 by forest destruction, deforestation, and cropland expansion.



### 3.5 Local hotspots of LCC

Regarding LC, more attention tends to be paid to global and regional LCC. At the local scale, we can further explore the hot spots of LCC and investigate the causes of such change by area. The main regions of LCC hotspots are shown in Fig. 15, where the depth of color represents a significant change.

- 365 In the north of Eurasia, forest has increased significantly, and that in Siberia has moved northward to the tundra regions, which is mainly the result of climate warming. The increase in temperature and soil moisture (thawing of the permafrost) has promoted plant growth (Berner et al., 2013).
- In northern North America, such as Alaska and the north of Canada, forest has also increased but the extent of the increase is weaker than that in North Eurasia. Studies have shown that this may be related to an insignificant temperature rise in North
- 370 America and even a slight cooling trend (Wang et al., 2011). In addition, fire disturbance in northern North America has interrupted forest succession (Alcaraz-Segura et al., 2010) and drought disasters in parts of the United States and Canada have increased tree mortality (Van Mantgem et al., 2009; Peng et al., 2011). These could also be possible reasons for the constant, or even decreasing, forest areas in these regions. In addition to climate warming, the decrease of cropland and increase of forest in the eastern part of the United States are related to forest restoration and management measures (Herrick et al., 2010).
- 375 In the Great Plains of Central North America, grassland has decreased and cropland has increased. It has been found that rising gasoline prices and the development of biofuels have led to increasing planting areas of corn and soybean in the United States (Lark et al., 2015; Wright and Wimberly, 2013).
- In most countries of South America, croplands have expanded substantially and forests have decreased significantly, especially in the southeastern part of the Amazon rainforest (shown in Fig. 16). This corresponds to the expansion of soybean planting
- 380 areas and the development of the cattle ranching industry (Zak et al., 2008; De Sy et al., 2015). In these regions, forest destruction and deforestation owing to human factors overtook the increase of vegetation caused by climate warming.
- In Southeast Asia, such as Cambodia, Vietnam, Indonesia and Malaysia, forest has also decreased significantly and cropland has increased. The expansion of cash crops (mainly oil palm) plantations and logging activities in Southeast Asia have led to serious destruction of primitive forests (Wilcove et al., 2013; Miettinen et al., 2011). Natural forest has either been turned into
- 385 artificial forest or cut down, resulting in huge loss of biodiversity and increased greenhouse gas emissions (Stibig et al., 2013).
- In Africa, forest in the northern part of the Congo Basin has expanded while forest in the southern Miombo forest belt has decreased (Devine et al., 2017). Studies have shown that the increase of forest in the northern part of Africa is related to low population growth, increased carbon dioxide and increased precipitation, while the decrease of forest in the southern part corresponds to high population growth (Brandt et al., 2017). It was also found that the rapid integration of global agricultural
- 390 markets in recent decades and subsequent urbanization has caused cropland loss and promoted large-scale tropical deforestation in South America and Southeast Asia (Ordway et al., 2017). Increasing land scarcity and stricter land use



regulations in South America and Southeast Asia may prompt export-oriented commodity crops to be outsourced to sub-Saharan Africa.

In China, forest has increased. In addition to carbon dioxide elevation and climate warming, human activities such as 395 afforestation and agricultural management (such as agricultural intensification) have also had a great impact on this trend (Piao et al., 2015;Guo and Gong, 2016). In addition, the increase in population and demand for food has led to the expansion of cropland in the Loess Plateau regions of China, while the increase in cropland in Northeast China has come mainly from wasteland reclamation (Liu et al., 2014).

Some grassland in Mongolia and Inner Mongolia of China showed a trend of degradation. Studies have shown overgrazing to 400 be the main cause of vegetation degradation in this region, while drought and soil erosion have played a secondary role (Yin et al., 2018). The obvious increase of grassland areas in the eastern part of the Qinghai-Tibet Plateau implies that the temperature rise has promoted vegetation growth in highly elevated regions, as vegetation growth in this region is usually limited by low temperatures (Wang et al., 2012). The decrease of grassland in central Asia and parts of Western Asia may be related to climate change where the area of land desertification has increased under the influence of drought (Cook et al., 2010).

405 In some parts of the former Soviet Union in Eastern Europe, a decrease of cropland and an increase of forest can be observed. Studies have found that a large number of cropland areas were abandoned after the dissolution of the Soviet Union and the transition from a planned economy to a market economy in these regions (Meyfroidt et al., 2016;Wertebach et al., 2017;Kuemmerle et al., 2011), which reflects the role of socio-economic systems in LCC.

#### 4 Discussions

410 Based on the accuracy assessment results, it can be seen that the global LC mapping products of 1982-2015, GLASS-GLC are reliable with high accuracies, and the global long-term mapping framework we designed is effective. Using GLASS-GLC CDRs in change analysis of LC can reflect a 34-year global landscape change pattern. Many phenomena and patterns can be confirmed by existing research, such as the expansion of tropical agricultural land, greening in the northern region, deforestation in the southern hemisphere and melting of snow and ice. In addition, we have assessed the impact of human 415 effects within different LC classes, and have further explored the causes of LCC in local hotspots, combined with field visits and literature reviews.

However, there are still deficiencies in the design of the mapping framework. First, the large grid size of  $0.05^{\circ}$ , due to the coarse spatial resolution, can only reflect the average change state of LC in a large area, thus many small-area phenomena cannot be well reflected (Gómez et al., 2016). For example, the reduction of much agricultural land is due to urbanization, and 420 the expansion of cities is usually sporadic. Although those changes are large at the global scale, they can hardly be reflected with  $0.05^{\circ}$  pixels. Moreover, due to the synthesis principle, the classification result of each pixel can only represent the class



with the largest proportion in area, and the information of remaining classes is ignored even though they can sometimes be more than 50 % in total. Such a neglect, due to the famous “Scale Effect” (Turner et al., 1989) can also cause great deviations in the final statistical summary of the LC area leading to uncertainties when compared with mapping results at finer resolutions.

425 Second, our sampling strategy for training has certain limitations. On one hand, since the training sample is generated from 30m global mapping results of more than 75 % accuracy, this will inevitably propagate and accumulate error to 5 km resolution. Of course, due to the higher signal-to-noise ratio of the high-resolution data, the sampling is still satisfactory compared to direct visual interpretation of the coarse resolution images. On the other hand, the training sample used is only from a single year of circa 2015. Although we have implemented a time series correction for the original input features and performed a 430 time-consistent post processing on the classification results, the effects of inter-annual fluctuations of the features cannot be completely avoided (Song et al., 2018a). On the other hand, according to the stable classification with limited sample theory (Gong et al., submitted), a representative sample collected in one year with less than 20 % in error should suffice in multiannual use at the global scale. Therefore, a multi-year sample set may not be as critical for multiannual classification provided the sample is better than 80 % accurate. In our case, although the source training data has an accuracy of 77 % (Gong et al., 2017), 435 we are not certain if the aggregated sample set exceeds an accuracy of 80 %. This needs further assessment.

For the generation of test samples, we have actually adopted the scale-up approach. That is to say, we first upscaled the 30m test samples set to 5 km by maximum area synthesis, which contains unavoidable errors because of scale transformation. The best way to verify the accuracy, of course, is to use a 0.05 ° test samples set directly derived at this resolution. However, due to the difficulty of visual interpretation in coarse scale and field investigation (Gong et al., 2013), establishing a sample library 440 at 5 km resolution is not easy. Thus, instead, we adopted the method of aggregation of 30m FROM-GLC\_v2 results to 5 km scale to generate samples. It is plausible to regard the selected test samples as “H-homo samples” that can be used for coarse resolution mapping. Although this method is feasible to a certain extent, there are inevitably errors.

We have eliminated wetland and impervious surface in our classification system. This is a tradeoff when working at the 5 km scale. Patches of wetland and impervious surface are usually small, and it is difficult to achieve a pixel size of 0.05 ° for many 445 situations, so the classification of the two types is extremely difficult. However, both are important LC types. Wetland is a transitional zone between terrestrial ecosystems and aquatic ecosystems (Davidson, 2014). The impervious surface can represent the urban area. In recent years, urban expansion has been a relatively significant phenomenon in global environmental change (Seto et al., 2011). Urban expansion reflects an important type of human activity, so the impervious surface is also one of the essential components to reflect anthropogenic influence though the total area of its change is usually small.

450 It should be pointed out that at a coarse resolution of 0.05 °, our definition of forest is more inclined to the tree canopy cover. Thus the changes in internal density of trees can also be reflected in the area change of forest, instead of just the stand-replacement type (Korhonen et al., 2006). In addition, the largest-class synthesis strategy we adopted also makes it unavoidable to include internal density change of various class, which in turn will further affect the classification and change area



calculation of forest class.

455 The result of our statistical summary shows that the global vegetated area increased significantly between 1982 and 2015, which is inconsistent with the results of FAO and some other global mapping products. This inconsistency originates from, on one hand, the above limitations of our designed mapping framework, and on the other hand, the statistics collected by FAO, and other census-based datasets, which are also affected by errors from many aspects, and its effectiveness is yet to be evaluated. Nevertheless, many studies can also confirm our results, such as (Song and Hansen, 2017; Song et al., 2018a; Piao et al., 460 2015; Pan et al., 2018) who have proved that the global vegetation area has increased with the increasing NDVI and LAI in time. To some extent, the sum of the global change area of forest, shrubland, and grassland is showing an increasing trend in our results, which can be seen as the sign of global vegetation growth.

In addition, because we are mainly depicting the natural biophysical properties of vegetated areas with limitation in resolution, some artificial features cannot be distinguished, such as plantations (rubber, oil palm, and various fruit trees) and natural forest, 465 which are uniformly included as forest in our classification system.

In the statistical analysis, although we have already conducted post-classification time-consistency processing for the original LC mapping results as much as possible, it is inevitable that there are still large fluctuations and interferences from various unknown factors unfavorable to the extraction of long-term trend of LCC. In order to ensure that the trend of the resulting time series is significant, we have to scale up the classification result from  $0.05^{\circ}$  to  $0.25^{\circ}$ , converting the original class label of 470 each  $0.05^{\circ}$  pixel to the class area ratio of  $0.25^{\circ}$  grid. The long-term time series of the area ratios is tested for statistical significance. However, in some cases this procedure will also be influenced by the “Scale Effect”.

In the analysis of anthropogenic influences, indirect effects of many human activities were ignored because the main objective was to include the effects of directly visible human activities. For example, human activities increase the concentration of carbon dioxide in the atmosphere, which in turn affects the global climate, leading to higher temperature, and thus increasing 475 vegetation coverage (Piao et al., 2006; Bonan, 2008). This pathway of action is indirect, but it is difficult to reflect in the human impact data we use, which results in an underestimation of the assessment of anthropogenic influences.

GLASS-GLCs contain more detailed LC classes, longer temporal coverage (34 years), high consistency, which meet the requirement for CDR. GLASS-GLC CDRs are the first collection of global LC dynamics of 5 km, and fill the existing gap for high-reliability and consistency of long-term general purpose global LC products. In addition, our strategy of generating 480 samples from high-resolution classification products can greatly reduce the cost and investment of sample collection, and can flexibly and effectively be extended to other coarse-resolution LC mapping tasks in the future.

In the future, with the advancement of technology and the accumulation of remote sensing datasets, the use of remote sensing products for LC mapping with higher resolution and longer time series will undoubtedly better reflect the global LC and its changes. However, under limited conditions, we can consider using coarse-resolution satellite data to determine the locations 485 of potential rapid change, and then use high-resolution data in these hotspots to accurately estimate the rate and mode of change.



Moreover, it is necessary to establish a multi-year sample library to assess the impact of inter-annual fluctuations in features on the accuracy of change characterization and analysis. Wetland and impervious surface are LC classes that have extremely high value. It would be useful to supplement the mapping and change analysis of these two classes when suitable data become available. For the analysis of global LCC, systematic and in-depth attribution analysis and research can be further carried out.

490 In addition, the development of LC ratio mapping products (similar to VCF products) with techniques of soft classification, rather than hard classification, especially for the case of coarse resolution, should be considered.

## 5 Data availability

GLASS-GLC products at 5 km resolution from 1982 to 2015 are available to the public in the TIFF format at <https://doi.org/10.1594/PANGAEA.898096> (Liu et al., 2019).

495 GLASS CDRs were provided by Beijing Normal University Data Center (<http://glass-product.bnu.edu.cn/>, last access: 27 December 2018). VCF products were obtained from the Land Processes Distributed Active Archive Center (<https://lpdaac.usgs.gov/>, last access: 20 December 2018). GMTED2010 were acquired from Google Earth Engine (<https://code.earthengine.google.com/>, last access: 24 December 2018). Geo-Wiki points came from the human impact campaign (<https://doi.pangaea.de/10.1594/PANGAEA.869680>, last access: 30 November 2018). Eco-region data were 500 obtained from the FAO global eco-region dataset (<http://www.fao.org/geonetwork/srv/en/metadata.show?CurrTab=simple&id=1255>, last access: 3 December 2018).

## 6 Conclusions

In order to better reflect the global land changes, continuous and dynamic monitoring of global LC is necessary. We built 505 GLASS-GLC, the first CDRs for global LC on the GEE platform. It can capture the global LCC information from 1982 to 2015. Compared to previous global LC products, GLASS-GLC products cover a longer time period and have higher consistency and more detailed classes. Our entire mapping framework is based on FROM-GLC\_v2, including the classification system and high-quality H-homo sample generation.

Based on over ten thousand independent test samples units from both the FROM-GLC sample set and FLUXNET site data, the average overall accuracy of GLASS-GLC was shown to exceed 80 %. Using inter-comparisons with other global LC 510 products of different resolutions from various data sources, we verified the effectiveness and reliability of GLASS-GLC from different perspectives. Systematic uncertainty analysis was also performed on a global scale based on the results of the accuracy assessment and its geographical distribution. This shows that GLASS-GLC CDR products have relatively low uncertainty in most parts of the world. Our results also indicate that GLASS CDRs have potential for multi-class LC mapping and can provide more than enough features and information to distinguish different LC classes, with relatively strong temporal and spatial



515 consistency, which can produce extremely reliable change information.

Comprehensive spatiotemporal pattern analysis based on GLASS-GLC reflected and revealed many significant global LCC phenomena and patterns, such as deforestation and agricultural land expansion in the tropics, afforestation and forest expansion in the northern regions, etc. An analysis of the global LC conversion pattern from 1982 to 2015 revealed hot spots of LCC such as land degradation, forest restoration, reclamation and agricultural land abandonment.

520 Since anthropogenic influence has become one of the most important driving forces for LCC, especially after the industrial revolution, we quantified the level of human impact in areas of significant LCC. The results show that the average human impact level in areas of significant LCC are about 25.49 %, suggesting that anthropogenic influence plays a strong role in vegetation destruction, expansion of tropical agricultural land, and degradation of grassland areas, etc. Under the current global climate change scenario with significantly elevated GHG concentrations and temperature rises, this remarkable human impact 525 has also contributed to a noticeable greening trend of the Earth because of the effect of carbon dioxide fertilization.

Combined with field visits and literature reviews on local LCC hot spots, we can see that global LC is affected by the synergetic effect of many complicated and multi-faceted factors, including human activity, climate change, socio-economic policies, and the natural environment transition, etc., and such change could further influence global and regional climate, environment, biodiversity, etc.

530 With increasing economic globalization, LCC has increased. Based on GLASS-GLC, effective global LC and change analysis could be conducted, enhancing our understanding of global environmental change, and even mitigating its negative impact to some extent, which is also beneficial to the achievement of sustainable development goals.

#### Author contribution

PG conceived the research. HL and JW designed the experiments and HL carried out experiments. NC provided GEE support.

535 SL provided data. HL prepared the manuscript with contributions from all co-authors.

#### Competing interests

The authors declare that they have no conflict of interest.

#### Acknowledgements

This work is partially supported by the National Key Research and Development Program of China (NO.2016YFA0600103),

540 a donation made by Delos Living LLC, and the Cyrus Tang Foundation.



## References

- Achard, F., Eva, H. D., Mayaux, P., Stibig, H. J., and Belward, A.: Improved estimates of net carbon emissions from land cover change in the tropics for the 1990s, *Global Biogeochemical Cycles*, 18, <https://doi.org/10.1029/2003GB002142>, 2004.
- Aide, T. M., Clark, M. L., Grau, H. R., López-Carr, D., Levy, M. A., Redo, D., Bonilla-Moheno, M., Riner, G., Andrade-Núñez, M. J., and Muñiz, M.: Deforestation and reforestation of Latin America and the Caribbean (2001–2010), *Biotropica*, 45, 262–271, <https://doi.org/10.1111/j.1744-7429.2012.00908.x>, 2013.
- Alcaraz-Segura, D., Chuvieco, E., Epstein, H. E., Kasischke, E. S., and Trishchenko, A.: Debating the greening vs. browning of the North American boreal forest: differences between satellite datasets, *Global Change Biology*, 16, 760–770, <https://doi.org/10.1111/j.1365-2486.2009.01956.x>, 2010.
- Andrew K., S., Nathalie, P., Nicholas C., C., Gary N., G., Matthew, H., Richard, L., Caspar A., M., Brian, O. C., Marc, P., and Henrique Miguel, P.: Environmental science: Agree on biodiversity metrics to track from space, *Nature*, 523, 403–405, <https://doi.org/10.1038/523403a>, 2015.
- Bai, Z. G., Dent, D. L., Olsson, L., and Schaepman, M. E.: Proxy global assessment of land degradation, Soil use and management, 24, 223–234, <https://doi.org/10.1111/j.1475-2743.2008.00169.x>, 2008.
- Ban, Y., Gong, P., and Gini, C.: Global land cover mapping using Earth observation satellite data: Recent progresses and challenges, *ISPRS journal of photogrammetry and remote sensing*, 103, 1–6, <https://doi.org/10.1016/j.isprsjprs.2015.01.001>, 2015.
- Barbier, E. B.: Explaining agricultural land expansion and deforestation in developing countries, *American Journal of Agricultural Economics*, 86, 1347–1353, <https://doi.org/10.1111/j.0002-9092.2004.00688.x>, 2004.
- Bartholome, E., and Belward, A. S.: GLC2000: a new approach to global land cover mapping from Earth observation data, *International Journal of Remote Sensing*, 26, 1959–1977, <https://doi.org/10.1080/01431160412331291297>, 2005.
- Bellwood, D. R., Hoey, A. S., and Hughes, T. P.: Human activity selectively impacts the ecosystem roles of parrotfishes on coral reefs, *Proceedings of the Royal Society B: Biological Sciences*, 279, 1621–1629, <https://doi.org/10.1098/rspb.2011.1906>, 2011.
- Berner, L. T., Beck, P. S. A., Bunn, A. G., and Goetz, S. J.: Plant response to climate change along the forest-tundra ecotone in northeastern Siberia, *Global Change Biology*, 19, 3449–3462, <https://doi.org/10.1111/gcb.12304>, 2013.
- Bonan, G. B.: Forests and climate change: forcings, feedbacks, and the climate benefits of forests, *Science*, 320, 1444–1449, <https://doi.org/10.1126/science.1155121>, 2008.
- Brandt, M., Rasmussen, K., Peñuelas, J., Tian, F., Schurgers, G., Verger, A., Mertz, O., Palmer, J. R. B., and Fensholt, R.: Human population growth offsets climate-driven increase in woody vegetation in sub-Saharan Africa, *Nature ecology & evolution*, 1, 0081, <https://doi.org/10.1038/s41559-017-0081>, 2017.
- Brink, A. B., and Eva, H. D.: Monitoring 25 years of land cover change dynamics in Africa: A sample based remote sensing approach, *Applied Geography*, 29, 501–512, <https://doi.org/10.1016/j.apgeog.2008.10.004>, 2009.
- Buermann, W., Parida, B., Jung, M., MacDonald, G. M., Tucker, C. J., and Reichstein, M.: Recent shift in Eurasian boreal forest greening response may be associated with warmer and drier summers, *Geophysical Research Letters*, 41, 1995–2002, <https://doi.org/10.1002/2014GL059450>, 2014.
- Cao, C., Xiong, X., Wu, A., and Wu, X.: Assessing the consistency of AVHRR and MODIS L1B reflectance for generating fundamental climate data records, *Journal of Geophysical Research: Atmospheres*, 113, <https://doi.org/10.1029/2007JD009363>, 2008.
- Chen, Y., Ge, Y., Heuvelink, G. B. M., An, R., and Chen, Y.: Object-based superresolution land-cover mapping from remotely sensed imagery, *IEEE Transactions on Geoscience and Remote Sensing*, 56, 328–340, <https://doi.org/10.1109/TGRS.2017.2747624>, 2018.
- Cheng, J., Liang, S., Verhoef, W., Shi, L., and Liu, Q.: Estimating the Hemispherical Broadband Longwave Emissivity of Global Vegetated Surfaces Using a Radiative Transfer Model, *IEEE Transactions on Geoscience and Remote Sensing*, 54, 905–917, <https://doi.org/10.1109/TGRS.2015.2469535>, 2016.
- Cihlar, J.: Land cover mapping of large areas from satellites: status and research priorities, *International Journal of Remote Sensing*, 21, 1093–1114, <https://doi.org/10.1080/014311600210092>, 2000.



- Claussen, M., Brovkin, V., and Ganopolski, A.: Biogeophysical versus biogeochemical feedbacks of large-scale land cover change, *Geophysical research letters*, 28, 1011-1014, <https://doi.org/10.1029/2000GL012471>, 2001.
- 590 Cohen, W. B., Yang, Z., Healey, S. P., Kennedy, R. E., and Gorelick, N.: A LandTrendr multispectral ensemble for forest disturbance detection, *Remote Sensing of Environment*, 205, 131-140, <https://doi.org/10.1016/j.rse.2017.11.015>, 2018.
- Cook, E. R., Anchukaitis, K. J., Buckley, B. M., D'Arrigo, R. D., Jacoby, G. C., and Wright, W. E.: Asian monsoon failure and megadrought during the last millennium, *Science*, 328, 486-489, <https://doi.org/10.1126/science.1185188>, 2010.
- 595 Cramer, W., Bondeau, A., Woodward, F. I., Prentice, I. C., Betts, R. A., Brovkin, V., Cox, P. M., Fisher, V., Foley, J. A., and Friend, A. D.: Global response of terrestrial ecosystem structure and function to CO<sub>2</sub> and climate change: results from six dynamic global vegetation models, *Global change biology*, 7, 357-373, <https://doi.org/10.1046/j.1365-2486.2001.00383.x>, 2001.
- Dangal, S. R. S., Tian, H., Lu, C., Pan, S., Pederson, N., and Hessl, A.: Synergistic effects of climate change and grazing on net primary production of Mongolian grasslands, *Ecosphere*, 7, e01274, <https://doi.org/10.1002/ecs2.1274>, 2016.
- 600 Davidson, N. C.: How much wetland has the world lost? Long-term and recent trends in global wetland area, *Marine and Freshwater Research*, 65, 934-941, <https://doi.org/10.1071/MF14173>, 2014.
- De Sy, V., Herold, M., Achard, F., Beuchle, R., Clevers, J., Lindquist, E., and Verchot, L.: Land use patterns and related carbon losses following deforestation in South America, *Environmental Research Letters*, 10, 124004, <https://doi.org/10.1088/1748-9326/10/12/124004>, 2015.
- 605 DeFries, R. S., Hansen, M., Townshend, J. R. G., and Sohlberg, R.: Global land cover classifications at 8 km spatial resolution: the use of training data derived from Landsat imagery in decision tree classifiers, *International Journal of Remote Sensing*, 19, 3141-3168, <https://doi.org/10.1080/014311698214235>, 1998.
- DeFries, R. S., Field, C. B., Fung, I., Collatz, G. J., and Bounoua, L.: Combining satellite data and biogeochemical models to estimate global effects of human-induced land cover change on carbon emissions and primary productivity, *Global Biogeochemical Cycles*, 13, 803-815, <https://doi.org/10.1029/1999GB900037>, 1999.
- 610 Devine, A. P., McDonald, R. A., Quaife, T., and Maclean, I. M. D.: Determinants of woody encroachment and cover in African savannas, *Oecologia*, 183, 939-951, <https://doi.org/10.1007/s00442-017-3807-6>, 2017.
- Dubovik, O., Menz, G., and Khamzina, A.: Trend analysis of MODIS time-series using different vegetation indices for monitoring of cropland degradation and abandonment in Central Asia, 6589-6592.
- 615 Feng, D., Yu, L., Zhao, Y., Cheng, Y., Xu, Y., Li, C., and Gong, P.: A multiple dataset approach for 30-m resolution land cover mapping: a case study of continental Africa, *International Journal of Remote Sensing*, 39, 3926-3938, <https://doi.org/10.1080/01431161.2018.1452073>, 2018.
- Friedl, M. A., Sulla-Menashe, D., Tan, B., Schneider, A., Ramankutty, N., Sibley, A., and Huang, X.: MODIS Collection 5 global land cover: Algorithm refinements and characterization of new datasets, *Remote Sensing of Environment*, 114, 168-182, <https://doi.org/10.1016/j.rse.2009.08.016>, 2010.
- Fritz, S., See, L., van der Velde, M., Nalepa, R. A., Perger, C., Schill, C., McCallum, I., Schepaschenko, D., Kraxner, F., and Cai, X.: Downgrading recent estimates of land available for biofuel production, *Environmental Science & Technology*, 47, 1688-1694, <https://doi.org/10.1021/es303141h>, 2013.
- 620 Fritz, S., See, L., Perger, C., McCallum, I., Schill, C., Schepaschenko, D., Duerauer, M., Karner, M., Dresel, C., and Laso-Bayas, J.-C.: A global dataset of crowdsourced land cover and land use reference data, *Scientific data*, 4, 170075, <https://doi.org/10.1038/sdata.2017.75>, 2017.
- Fuller, R. M., Smith, G. M., and Devereux, B. J.: The characterisation and measurement of land cover change through remote sensing: problems in operational applications?, *International Journal of Applied Earth Observation and Geoinformation*, 4, 243-253, [https://doi.org/10.1016/S0303-2434\(03\)00004-7](https://doi.org/10.1016/S0303-2434(03)00004-7), 2003.
- 630 Gallego, F. J.: Remote sensing and land cover area estimation, *International Journal of Remote Sensing*, 25, 3019-3047, <https://doi.org/10.1080/01431160310001619607>, 2004.
- Gibbard, S., Caldeira, K., Bala, G., Phillips, T. J., and Wickett, M.: Climate effects of global land cover change, *Geophysical Research Letters*, 32, <https://doi.org/10.1029/2005GL024550>, 2005.
- Gibbs, H. K., Ruesch, A. S., Achard, F., Clayton, M. K., Holmgren, P., Ramankutty, N., and Foley, J. A.: Tropical forests were



- 635 the primary sources of new agricultural land in the 1980s and 1990s, Proceedings of the National Academy of Sciences, 107, 16732-16737, <https://doi.org/10.1073/pnas.0910275107>, 2010.
- Gómez, C., White, J. C., and Wulder, M. A.: Optical remotely sensed time series data for land cover classification: A review, ISPRS Journal of Photogrammetry and Remote Sensing, 116, 55-72, <https://doi.org/10.1016/j.isprsjprs.2016.03.008>, 2016.
- Gong, P.: Accuracy assessment of global land cover datasets based on global field stations, Progress in Natural Science, 19, 640 754-759, 2009.
- Gong, P.: Remote sensing of environmental change over China: A review, Chinese Science Bulletin, 57, 2793-2801, <https://doi.org/10.1007/s11434-012-5268-y>, 2012.
- Gong, P., Wang, J., Yu, L., Zhao, Y., Zhao, Y., Liang, L., Niu, Z., Huang, X., Fu, H., and Liu, S.: Finer resolution observation and monitoring of global land cover: First mapping results with Landsat TM and ETM+ data, International Journal of Remote Sensing, 34, 2607-2654, <https://doi.org/10.1080/01431161.2012.748992>, 2013.
- Gong, P., Wang, J., Li, C., Ji, L., Huang, H., Clinton, N., and Cheng, Y.: Automated Global Land Cover Mapping – FROM-GLC Version 2: the production of the 30 m circa 2015 global land cover map, Product Report. <http://data.ess.tsinghua.edu.cn/>, Accessed January 31, 2019, 2017.
- Gong, P., Liu, H., Zhang, M., Li, C., Wang, J., Huang, H., Clinton, N., Ji, L., Li, W., Bai, Y., Chen, B., Xu, B., Zhu, Z., Yuan, C., Suen, H. P., Guo, J., Xu, N., Li, W., Zhao, Y., Yang, J., Yu, C., Wang, X., Fu, H., Yu, L., Dronova, I., Hui, F., Cheng, X., Shi, X., Xiao, F., Liu, Q., and Song, L.: Stable classification with limited sample: transferring a 30-m resolution sample set collected in 2015 to mapping 10-m resolution global land cover in 2017, submitted.
- Gorelick, N., Hancher, M., Dixon, M., Ilyushchenko, S., Thau, D., and Moore, R.: Google Earth Engine: Planetary-scale geospatial analysis for everyone, Remote Sensing of Environment, 202, 18-27, <https://doi.org/10.1016/j.rse.2017.06.031>, 2017.
- 655 Grekousis, G., Mountrakis, G., and Kavouras, M.: An overview of 21 global and 43 regional land-cover mapping products, International Journal of Remote Sensing, 36, 5309-5335, <https://doi.org/10.1080/01431161.2015.1093195>, 2015.
- Guo, J., and Gong, P.: Forest cover dynamics from Landsat time-series data over Yan'an city on the Loess Plateau during the Grain for Green Project, International Journal of Remote Sensing, 37, 4101-4118, <https://doi.org/10.1080/01431161.2016.1207264>, 2016.
- 660 Hansen, M. C., DeFries, R. S., Townshend, J. R. G., and Sohlberg, R.: Global land cover classification at 1 km spatial resolution using a classification tree approach, International journal of remote sensing, 21, 1331-1364, <https://doi.org/10.1080/014311600210209>, 2000.
- Hansen, M. C., Potapov, P. V., Moore, R., Hancher, M., Turubanova, S. A. A., Tyukavina, A., Thau, D., Stehman, S. V., Goetz, S. J., and Loveland, T. R.: High-resolution global maps of 21st-century forest cover change, science, 342, 850-853, <https://doi.org/10.1126/science.1244693>, 2013.
- Herold, M., Mayaux, P., Woodcock, C. E., Baccini, A., and Schmullius, C.: Some challenges in global land cover mapping: An assessment of agreement and accuracy in existing 1 km datasets, Remote Sensing of Environment, 112, 2538-2556, <https://doi.org/10.1016/j.rse.2007.11.013>, 2008.
- Herrick, J. E., Lessard, V. C., Spaeth, K. E., Shaver, P. L., Dayton, R. S., Pyke, D. A., Jolley, L., and Goebel, J. J.: National ecosystem assessments supported by scientific and local knowledge, Frontiers in Ecology and the Environment, 8, 403-408, <https://doi.org/10.1890/100017>, 2010.
- Hollmann, R., Merchant, C. J., Saunders, R., Downy, C., Buchwitz, M., Cazenave, A., Chuvieco, E., Defourny, P., de Leeuw, G., and Forsberg, R.: The ESA climate change initiative: Satellite data records for essential climate variables, Bulletin of the American Meteorological Society, 94, 1541-1552, <https://doi.org/10.1175/BAMS-D-11-00254.1>, 2013.
- 675 Homer, C., Huang, C., Yang, L., Wylie, B., and Coan, M.: Development of a 2001 national land-cover database for the United States, Photogrammetric Engineering & Remote Sensing, 70, 829-840, <https://doi.org/10.14358/PERS.70.7.829>, 2004.
- Hosonuma, N., Herold, M., De Sy, V., De Fries, R. S., Brockhaus, M., Verchot, L., Angelsen, A., and Romijn, E.: An assessment of deforestation and forest degradation drivers in developing countries, Environmental Research Letters, 7, 044009, <https://doi.org/10.1088/1748-9326/7/4/044009>, 2012.
- 680 Houghton, R. A., House, J. I., Pongratz, J., Van Der Werf, G. R., DeFries, R. S., Hansen, M. C., Quéré, C. L., and Ramankutty, N.: Carbon emissions from land use and land-cover change, Biogeosciences, 9, 5125-5142, <https://doi.org/10.5194/bg-9-5125-2012>, 2012.



2012, 2012.

Ji, L., Gong, P., Wang, J., Shi, J., and Zhu, Z.: Construction of the 500 m resolution daily global surface water change database (2001–2016), Water Resources Research, <https://doi.org/10.1029/2018WR023060>.

685 Kennedy, R. E., Yang, Z., and Cohen, W. B.: Detecting trends in forest disturbance and recovery using yearly Landsat time series: 1. LandTrendr—Temporal segmentation algorithms, Remote Sensing of Environment, 114, 2897–2910, <https://doi.org/10.1016/j.rse.2010.07.008>, 2010.

Korhonen, L., Korhonen, K. T., Rautiainen, M., and Stenberg, P.: Estimation of forest canopy cover: a comparison of field measurement techniques, Silva Fennica, 40, 577–588, <https://doi.org/10.14214/sf.315>, 2006.

690 Kuemmerle, T., Olofsson, P., Chaskovskyy, O., Baumann, M., Ostapowicz, K., Woodcock, C. E., Houghton, R. A., Hostert, P., Keeton, W. S., and Radeloff, V. C.: Post-Soviet farmland abandonment, forest recovery, and carbon sequestration in western Ukraine, Global Change Biology, 17, 1335–1349, <https://doi.org/10.1111/j.1365-2486.2010.02333.x>, 2011.

Lambin, E. F., Turner, B. L., Geist, H. J., Agbola, S. B., Angelsen, A., Bruce, J. W., Coomes, O. T., Dirzo, R., Fischer, G., and Folke, C.: The causes of land-use and land-cover change: moving beyond the myths, Global environmental change, 11, 261–269, [https://doi.org/10.1016/S0959-3780\(01\)00007-3](https://doi.org/10.1016/S0959-3780(01)00007-3), 2001.

Lambin, E. F., Geist, H., and Rindfuss, R. R.: Introduction: Local Processes with Global Impacts, in: Land-Use and Land-Cover Change: Local Processes and Global Impacts, edited by: Lambin, E. F., and Geist, H., Springer Berlin Heidelberg, Berlin, Heidelberg, 1–8, 2006.

Lark, T. J., Salmon, J. M., and Gibbs, H. K.: Cropland expansion outpaces agricultural and biofuel policies in the United States, Environmental Research Letters, 10, 044003, <https://doi.org/10.1088/1748-9326/10/4/044003>, 2015.

Lepers, E., Lambin, E. F., Janetos, A. C., DeFries, R., Achard, F., Ramankutty, N., and Scholes, R. J.: A synthesis of information on rapid land-cover change for the period 1981–2000, AIBS Bulletin, 55, 115–124, [https://doi.org/10.1641/0006-3568\(2005\)055\[0115:ASOIOR\]2.0.CO;2](https://doi.org/10.1641/0006-3568(2005)055[0115:ASOIOR]2.0.CO;2), 2005.

705 Li, C., Wang, J., Wang, L., Hu, L., and Peng, G.: Comparison of classification algorithms and training sample sizes in urban land classification with Landsat Thematic Mapper Imagery, Remote Sensing, 6, 964–983, <https://doi.org/10.3390/rs6020964>, 2014.

Li, C., Gong, P., Wang, J., Yuan, C., Hu, T., Wang, Q., Yu, L., Clinton, N., Li, M., and Guo, J.: An all-season sample database for improving land-cover mapping of Africa with two classification schemes, International Journal of Remote Sensing, 37, 4623–4647, <https://doi.org/10.1080/01431161.2016.1213923>, 2016.

710 Li, C., Gong, P., Wang, J., Zhu, Z., Biging, G. S., Yuan, C., Hu, T., Zhang, H., Wang, Q., Li, X., Liu, X., Xu, Y., Guo, J., Liu, C., Hackman, K. O., Zhang, M., Cheng, Y., Yu, L., Yang, J., Huang, H., and Clinton, N.: The first all-season sample set for mapping global land cover with Landsat-8 data, Science Bulletin, 62, 508–515, <https://doi.org/10.1016/j.scib.2017.03.011>, 2017.

715 Li, X., Zhou, Y., Zhu, Z., Liang, L., Yu, B., and Cao, W.: Mapping annual urban dynamics (1985–2015) using time series of Landsat data, Remote Sensing of Environment, 216, 674–683, <https://doi.org/10.1016/j.rse.2018.07.030>, 2018.

Liang, S., Zhao, X., Liu, S., Yuan, W., Cheng, X., Xiao, Z., Zhang, X., Liu, Q., Cheng, J., and Tang, H.: A long-term Global Land Surface Satellite (GLASS) data-set for environmental studies, International Journal of Digital Earth, 6, 5–33, <https://doi.org/10.1080/17538947.2013.805262>, 2013.

720 Liu, H., Gong, P., Wang, J., Clinton, N., Bai, Y., and Liang, S.: Annual Dynamics of Global Land Cover and its Long-term Changes from 1982 to 2015, <https://doi.org/10.1594/PANGAEA.898096>, 2019.

Liu, J., Liu, M., Deng, X., Zhuang, D., Zhang, Z., and Luo, D.: The land use and land cover change database and its relative studies in China, Journal of Geographical Sciences, 12, 275–282, <https://doi.org/10.1007/BF02837545>, 2002.

725 Liu, J., Liu, M., Tian, H., Zhuang, D., Zhang, Z., Zhang, W., Tang, X., and Deng, X.: Spatial and temporal patterns of China's cropland during 1990–2000: an analysis based on Landsat TM data, Remote sensing of Environment, 98, 442–456, <https://doi.org/10.1016/j.rse.2005.08.012>, 2005.

Liu, J., Kuang, W., Zhang, Z., Xu, X., Qin, Y., Ning, J., Zhou, W., Zhang, S., Li, R., and Yan, C.: Spatiotemporal characteristics, patterns, and causes of land-use changes in China since the late 1980s, Journal of Geographical Sciences, 24, 195–210, <https://doi.org/10.1007/s11442-014-1082-6>, 2014.



- Loveland, T. R., Reed, B. C., Brown, J. F., Ohlen, D. O., Zhu, Z., Yang, L., and Merchant, J. W.: Development of a global land cover characteristics database and IGBP DISCover from 1 km AVHRR data, International Journal of Remote Sensing, 21, 1303-1330, <https://doi.org/10.1080/014311600210191>, 2000.
- Macias-Fauria, M., Forbes, B. C., Zetterberg, P., and Kumpula, T.: Eurasian Arctic greening reveals teleconnections and the potential for structurally novel ecosystems, Nature Climate Change, 2, 613, <https://doi.org/10.1038/nclimate1558>, 2012.
- Mann, H. B.: Nonparametric tests against trend, Econometrica: Journal of the Econometric Society, 245-259, <http://dx.doi.org/10.2307/1907187>, 1945.
- Margono, B. A., Turubanova, S., Zhuravleva, I., Potapov, P., Tyukavina, A., Baccini, A., Goetz, S., and Hansen, M. C.: Mapping and monitoring deforestation and forest degradation in Sumatra (Indonesia) using Landsat time series data sets from 1990 to 2010, Environmental Research Letters, 7, 034010, <https://doi.org/10.1088/1748-9326/7/3/034010>, 2012.
- Marlon, J. R., Bartlein, P. J., Carcaillet, C., Gavin, D. G., Harrison, S. P., Higuera, P. E., Joos, F., Power, M. J., and Prentice, I. C.: Climate and human influences on global biomass burning over the past two millennia, Nature Geoscience, 1, 697, <https://doi.org/10.1038/ngeo313>, 2008.
- Matthews, H. D., Weaver, A. J., Meissner, K. J., Gillett, N. P., and Eby, M.: Natural and anthropogenic climate change: incorporating historical land cover change, vegetation dynamics and the global carbon cycle, Climate Dynamics, 22, 461-479, <https://doi.org/10.1007/s00382-004-0392-2>, 2004.
- Meyer, W. B., and Turner, B. L.: Human population growth and global land-use/cover change, Annual review of ecology and systematics, 23, 39-61, <https://doi.org/10.1146/annurev.es.23.110192.000351>, 1992.
- Meyfroidt, P., Schierhorn, F., Prischepov, A. V., Müller, D., and Kuemmerle, T.: Drivers, constraints and trade-offs associated with recultivating abandoned cropland in Russia, Ukraine and Kazakhstan, Global environmental change, 37, 1-15, <https://doi.org/10.1016/j.gloenvcha.2016.01.003>, 2016.
- Miettinen, J., Shi, C., and Liew, S. C.: Deforestation rates in insular Southeast Asia between 2000 and 2010, Global Change Biology, 17, 2261-2270, <https://doi.org/10.1111/j.1365-2486.2011.02398.x>, 2011.
- Myneni, R. B., Keeling, C. D., Tucker, C. J., Asrar, G., and Nemani, R. R.: Increased plant growth in the northern high latitudes from 1981 to 1991, Nature, 386, 698, <https://doi.org/10.1038/386698a0>, 1997.
- Oliver, M. A., and Webster, R.: Kriging: a method of interpolation for geographical information systems, International Journal of Geographical Information System, 4, 313-332, <https://doi.org/10.1080/02693799008941549>, 1990.
- Ordway, E. M., Asner, G. P., and Lambin, E. F.: Deforestation risk due to commodity crop expansion in sub-Saharan Africa, Environmental Research Letters, 12, 044015, <https://doi.org/10.1088/1748-9326/aa6509>, 2017.
- Pal, M.: Random forest classifier for remote sensing classification, International Journal of Remote Sensing, 26, 217-222, <https://doi.org/10.1080/01431160412331269698>, 2005.
- Pan, N., Feng, X., Fu, B., Wang, S., Ji, F., and Pan, S.: Increasing global vegetation browning hidden in overall vegetation greening: Insights from time-varying trends, Remote Sensing of Environment, 214, 59-72, <https://doi.org/10.1016/j.rse.2018.05.018>, 2018.
- Pan, Y., Birdsey, R. A., Fang, J., Houghton, R., Kauppi, P. E., Kurz, W. A., Phillips, O. L., Shvidenko, A., Lewis, S. L., and Canadell, J. G.: A large and persistent carbon sink in the world's forests, Science, 1201609, 2011.
- Park, T., Ganguly, S., Tømmervik, H., Euskirchen, E. S., Høgda, K.-A., Karlsen, S. R., Brovkin, V., Nemani, R. R., and Myneni, R. B.: Changes in growing season duration and productivity of northern vegetation inferred from long-term remote sensing data, Environmental Research Letters, 11, 084001, <https://doi.org/10.1088/1748-9326/11/8/084001>, 2016.
- Pekel, J.-F., Cottam, A., Gorelick, N., and Belward, A. S.: High-resolution mapping of global surface water and its long-term changes, Nature, 540, 418, <https://doi.org/10.1038/nature20584>, 2016.
- Peng, C., Ma, Z., Lei, X., Zhu, Q., Chen, H., Wang, W., Liu, S., Li, W., Fang, X., and Zhou, X.: A drought-induced pervasive increase in tree mortality across Canada's boreal forests, Nature climate change, 1, 467, <https://doi.org/10.1038/nclimate1293>, 2011.
- Piao, S., Friedlingstein, P., Ciais, P., Zhou, L., and Chen, A.: Effect of climate and CO<sub>2</sub> changes on the greening of the Northern Hemisphere over the past two decades, Geophysical Research Letters, 33, <https://doi.org/10.1029/2006GL028205>, 2006.
- Piao, S., Yin, G., Tan, J., Cheng, L., Huang, M., Li, Y., Liu, R., Mao, J., Myneni, R. B., and Peng, S.: Detection and attribution



of vegetation greening trend in China over the last 30 years, *Global Change Biology*, 21, 1601-1609, <https://doi.org/10.1111/gcb.12795>, 2015.

Pielke, R. A.: Land use and climate change, *Science*, 310, 1625-1626, <https://doi.org/10.1126/science.1120529>, 2005.

780 Pittman, K., Hansen, M. C., Becker-Reshef, I., Potapov, P. V., and Justice, C. O.: Estimating global cropland extent with multi-year MODIS data, *Remote Sensing*, 2, 1844-1863, <https://doi.org/10.3390/rs2071844>, 2010.

Qu, Y., Liu, Q., Liang, S., Wang, L., Liu, N., and Liu, S.: Direct-estimation algorithm for mapping daily land-surface broadband albedo from MODIS data, *IEEE Transactions on Geoscience and Remote sensing*, 52, 907-919, <https://doi.org/10.1109/TGRS.2013.2245670>, 2014.

785 Ramankutty, N., Graumlich, L., Achard, F., Alves, D., Chhabra, A., DeFries, R. S., Foley, J. A., Geist, H., Houghton, R. A., and Goldeijk, K. K.: Global land-cover change: Recent progress, remaining challenges, in: *Land-use and land-cover change*, Springer, 9-39, 2006.

Reyers, B., O'Farrell, P. J., Cowling, R. M., Ego, B. N., Le Maitre, D. C., and Vlok, J. H. J.: Ecosystem services, land-cover change, and stakeholders: finding a sustainable foothold for a semiarid biodiversity hotspot, *Ecology and Society*, 14, <http://www.ecologyandsociety.org/vol14/iss1/art38>, 2009.

790 Richardson, A. D., Keenan, T. F., Migliavacca, M., Ryu, Y., Sonnentag, O., and Toomey, M.: Climate change, phenology, and phenological control of vegetation feedbacks to the climate system, *Agricultural and Forest Meteorology*, 169, 156-173, <https://doi.org/10.1016/j.agrformet.2012.09.012>, 2013.

Rindfuss, R. R., Walsh, S. J., Turner, B. L., Fox, J., and Mishra, V.: Developing a science of land change: challenges and methodological issues, *Proceedings of the National Academy of Sciences*, 101, 13976-13981, <https://doi.org/10.1073/pnas.0401545101>, 2004.

Rodriguez-Galiano, V. F., Ghimire, B., Rogan, J., Chica-Olmo, M., and Rigol-Sanchez, J. P.: An assessment of the effectiveness of a random forest classifier for land-cover classification, *ISPRS Journal of Photogrammetry and Remote Sensing*, 67, 93-104, <https://doi.org/10.1016/j.isprsjprs.2011.11.002>, 2012.

800 Rogan, J., and Chen, D.: Remote sensing technology for mapping and monitoring land-cover and land-use change, *Progress in planning*, 61, 301-325, [https://doi.org/10.1016/S0305-9006\(03\)00066-7](https://doi.org/10.1016/S0305-9006(03)00066-7), 2004.

Running, S. W.: Ecosystem disturbance, carbon, and climate, *Science*, 321, 652-653, <https://doi.org/10.1126/science.1159607>, 2008.

805 Schneider, A., Friedl, M. A., and Potere, D.: Mapping global urban areas using MODIS 500-m data: New methods and datasets based on 'urban ecoregions', *Remote Sensing of Environment*, 114, 1733-1746, <https://doi.org/10.1016/j.rse.2010.03.003>, 2010.

Sen, P. K.: Estimates of the regression coefficient based on Kendall's tau, *Journal of the American statistical association*, 63, 1379-1389, <https://doi.org/10.1080/01621459.1968.10480934>, 1968.

Seto, K. C., Frakias, M., Güneralp, B., and Reilly, M. K.: A meta-analysis of global urban land expansion, *PloS one*, 6, e23777, <https://doi.org/10.1371/journal.pone.0023777>, 2011.

810 Simons, H., Soto, X., Zhu, Z., Singh, K. D., Bellan, M.-F., Iremonger, S., Hirvonen, H., Smith, B., Watson, V., and Tosi, J.: Global ecological zoning for the global forest resources assessment 2000-final report, 2001.

Song, X.-P., Hansen, M. C., Stehman, S. V., Potapov, P. V., Tyukavina, A., Vermote, E. F., and Townshend, J. R.: Global land change from 1982 to 2016, *Nature*, 560, 639, <https://doi.org/10.1038/s41586-018-0411-9>, 2018a.

Song, X. P., and Hansen, M.: Satellite assessment of increasing tree cover 1982-2016, *Agu Fall Meeting*, 2017,

815 Song, Z., Liang, S., Wang, D., Zhou, Y., and Jia, A.: Long-term record of top-of-atmosphere albedo over land generated from AVHRR data, *Remote Sensing of Environment*, 211, 71-88, <https://doi.org/10.1016/j.rse.2018.03.044>, 2018b.

Sterling, S. M., Ducharne, A., and Polcher, J.: The impact of global land-cover change on the terrestrial water cycle, *Nature Climate Change*, 3, 385, <https://doi.org/10.1038/nclimate1690>, 2013.

820 Stibig, H. J., Achard, F., Carboni, S., Raši, R., and Miettinen, J.: Change in tropical forest cover of Southeast Asia from 1990 to 2010, *Biogeosciences Discussions*, 10, 12625-12653, <https://doi.org/10.5194/bgd-10-12625-2013>, 2013.

Tucker, C. J., Townshend, J. R. G., and Goff, T. E.: African land-cover classification using satellite data, *Science*, 227, 369-375, <https://doi.org/10.1126/science.227.4685.369>, 1985.



- Turner, B. L., Lambin, E. F., and Reenberg, A.: The emergence of land change science for global environmental change and sustainability, *Proceedings of the National Academy of Sciences*, 104, 20666-20671, <https://doi.org/10.1073/pnas.0704119104>, 2007.
- 825 Turner, M. G., O'Neill, R. V., Gardner, R. H., and Milne, B. T.: Effects of changing spatial scale on the analysis of landscape pattern, *Landscape ecology*, 3, 153-162, <https://doi.org/10.1007/BF00131534>, 1989.
- Van Mantgem, P. J., Stephenson, N. L., Byrne, J. C., Daniels, L. D., Franklin, J. F., Fulé, P. Z., Harmon, M. E., Larson, A. J., Smith, J. M., and Taylor, A. H.: Widespread increase of tree mortality rates in the western United States, *Science*, 323, 521-524, <https://doi.org/10.1126/science.1165000>, 2009.
- 830 Verburg, P. H., Van De Steeg, J., Veldkamp, A., and Willemen, L.: From land cover change to land function dynamics: a major challenge to improve land characterization, *Journal of environmental management*, 90, 1327-1335, <https://doi.org/10.1016/j.jenvman.2008.08.005>, 2009.
- Wang, C., Gao, Q., Wang, X., and Yu, M.: Spatially differentiated trends in urbanization, agricultural land abandonment and 835 reclamation, and woodland recovery in Northern China, *Scientific reports*, 6, 37658, <https://doi.org/10.1038/srep37658>, 2016.
- Wang, J., Zhao, Y., Li, C., Yu, L., Liu, D., and Gong, P.: Mapping global land cover in 2001 and 2010 with spatial-temporal consistency at 250 m resolution, *ISPRS Journal of Photogrammetry and Remote Sensing*, 103, 38-47, <https://doi.org/10.1016/j.isprsjprs.2014.03.007>, 2015.
- 840 Wang, S., Duan, J., Xu, G., Wang, Y., Zhang, Z., Rui, Y., Luo, C., Xu, B., Zhu, X., and Chang, X.: Effects of warming and grazing on soil N availability, species composition, and ANPP in an alpine meadow, *Ecology*, 93, 2365-2376, <https://doi.org/10.1890/11-1408.1>, 2012.
- Wang, X., Piao, S., Ciais, P., Li, J., Friedlingstein, P., Koven, C., and Chen, A.: Spring temperature change and its implication 845 in the change of vegetation growth in North America from 1982 to 2006, *Proceedings of the National Academy of Sciences*, 108, 1240-1245, <https://doi.org/10.1073/pnas.1014425108>, 2011.
- Wardlow, B. D., and Egbert, S. L.: Large-area crop mapping using time-series MODIS 250 m NDVI data: An assessment for the US Central Great Plains, *Remote sensing of environment*, 112, 1096-1116, <https://doi.org/10.1016/j.rse.2007.07.019>, 2008.
- Wertebach, T. M., Hölszel, N., Kämpf, I., Yurtaev, A., Tupitsin, S., Kiehl, K., Kamp, J., and Kleinebecker, T.: Soil carbon sequestration due to post-Soviet cropland abandonment: estimates from a large-scale soil organic carbon field inventory, *Global change biology*, 23, 3729-3741, <https://doi.org/10.1111/gcb.13650>, 2017.
- 850 Wilcove, D. S., Giam, X., Edwards, D. P., Fisher, B., and Koh, L. P.: Navjot's nightmare revisited: logging, agriculture, and biodiversity in Southeast Asia, *Trends in ecology & evolution*, 28, 531-540, <https://doi.org/10.1016/j.tree.2013.04.005>, 2013.
- Wood, E. F., Roundy, J. K., Troy, T. J., Van Beek, L. P. H., Bierkens, M. F. P., Blyth, E., de Roo, A., Döll, P., Ek, M., and Famiglietti, J.: Hyperresolution global land surface modeling: Meeting a grand challenge for monitoring Earth's terrestrial water, *Water Resources Research*, 47, <https://doi.org/10.1029/2010WR010090>, 2011.
- 855 Wright, C. K., and Wimberly, M. C.: Recent land use change in the Western Corn Belt threatens grasslands and wetlands, *Proceedings of the National Academy of Sciences*, 110, 4134-4139, <https://doi.org/10.1073/pnas.1215404110>, 2013.
- Wulder, M. A., White, J. C., Goward, S. N., Masek, J. G., Irons, J. R., Herold, M., Cohen, W. B., Loveland, T. R., and Woodcock, C. E.: Landsat continuity: Issues and opportunities for land cover monitoring, *Remote Sensing of Environment*, 112, 955-969, <https://doi.org/10.1016/j.rse.2007.07.004>, 2008.
- 860 Xiao, Z., Liang, S., Sun, R., Wang, J., and Jiang, B.: Estimating the fraction of absorbed photosynthetically active radiation from the MODIS data based GLASS leaf area index product, *Remote Sensing of Environment*, 171, 105-117, <https://doi.org/10.1016/j.rse.2015.10.016>, 2015.
- Xiao, Z., Liang, S., Wang, J., Xiang, Y., Zhao, X., and Song, J.: Long-time-series global land surface satellite leaf area index Product Derived From MODIS and AVHRR Surface Reflectance, *IEEE Trans. Geoscience and Remote Sensing*, 54, 5301-5318, <https://doi.org/10.1109/TGRS.2016.2560522>, 2016.
- 865 Xie, S., Liu, L., Zhang, X., and Chen, X.: Annual land-cover mapping based on multi-temporal cloud-contaminated landsat images, *International Journal of Remote Sensing*, 1-23, <https://doi.org/10.1080/01431161.2018.1553320>, 2018.
- Xu, Y., Yu, L., Zhao, F. R., Cai, X., Zhao, J., Lu, H., and Gong, P.: Tracking annual cropland changes from 1984 to 2016 using time-series Landsat images with a change-detection and post-classification approach: Experiments from three sites in Africa,



- 870 Remote Sensing of Environment, 218, 13-31, <https://doi.org/10.1016/j.rse.2018.09.008>, 2018.  
Yang, J., Peng, G., Rong, F., Zhang, M., Chen, J., Liang, S., Bing, X., Shi, J., and Dickinson, R.: The role of satellite remote sensing in climate change studies, *Nature Climate Change*, 3, 875-883, <https://doi.org/10.1038/nclimate1908>, 2013.
- 875 Yao, Y., Liang, S., Li, X., Hong, Y., Fisher, J. B., Zhang, N., Chen, J., Cheng, J., Zhao, S., and Zhang, X.: Bayesian multimodel estimation of global terrestrial latent heat flux from eddy covariance, meteorological, and satellite observations, *Journal of Geophysical Research: Atmospheres*, 119, 4521-4545, <https://doi.org/10.1002/2013JD020864>, 2014.
- Yin, H., Pflugmacher, D., Li, A., Li, Z., and Hostert, P.: Land use and land cover change in Inner Mongolia-understanding the effects of China's re-vegetation programs, *Remote Sensing of Environment*, 204, 918-930, <https://doi.org/10.1016/j.rse.2017.08.030>, 2018.
- 880 Ying, Q., Hansen, M. C., Potapov, P. V., Tyukavina, A., Wang, L., Stehman, S. V., Moore, R., and Hancher, M.: Global bare ground gain from 2000 to 2012 using Landsat imagery, *Remote sensing of environment*, 194, 161-176, <https://doi.org/10.1016/j.rse.2017.03.022>, 2017.
- 885 Yuan, F., Sawaya, K. E., Loeffelholz, B. C., and Bauer, M. E.: Land cover classification and change analysis of the Twin Cities (Minnesota) Metropolitan Area by multitemporal Landsat remote sensing, *Remote sensing of Environment*, 98, 317-328, <https://doi.org/10.1016/j.rse.2005.08.006>, 2005.
- 890 Yuan, W., Liu, S., Yu, G., Bonnefond, J.-M., Chen, J., Davis, K., Desai, A. R., Goldstein, A. H., Gianelle, D., and Rossi, F.: Global estimates of evapotranspiration and gross primary production based on MODIS and global meteorology data, *Remote Sensing of Environment*, 114, 1416-1431, <https://doi.org/10.1016/j.rse.2010.01.022>, 2010.
- Zak, M. R., Cabido, M., Cáceres, D., and Díaz, S.: What drives accelerated land cover change in central Argentina? Synergistic consequences of climatic, socioeconomic, and technological factors, *Environmental Management*, 42, 181-189, <https://doi.org/10.1007/s00267-008-9101-y>, 2008.
- 895 Zhang, G., Biradar, C. M., Xiao, X., Dong, J., Zhou, Y., Qin, Y., Zhang, Y., Liu, F., Ding, M., and Thomas, R. J.: Exacerbated grassland degradation and desertification in Central Asia during 2000–2014, *Ecological Applications*, 28, 442-456, <https://doi.org/10.1002/eaap.1660>, 2018.
- Zhang, Q., and Seto, K. C.: Mapping urbanization dynamics at regional and global scales using multi-temporal DMSP/OLS nighttime light data, *Remote Sensing of Environment*, 115, 2320-2329, <https://doi.org/10.1016/j.rse.2011.04.032>, 2011.
- Zhao, M., Pitman, A. J., and Chase, T.: The impact of land cover change on the atmospheric circulation, *Climate Dynamics*, 17, 467-477, <https://doi.org/10.1038/nclimate3004>, 2001.
- 900 Zhu, Z., Piao, S., Myneni, R. B., Huang, M., Zeng, Z., Canadell, J. G., Ciais, P., Sitch, S., Friedlingstein, P., and Arneth, A.: Greening of the Earth and its drivers, *Nature Climate Change*, 6, 791-795, <https://doi.org/10.1007/PL00013740>, 2016.

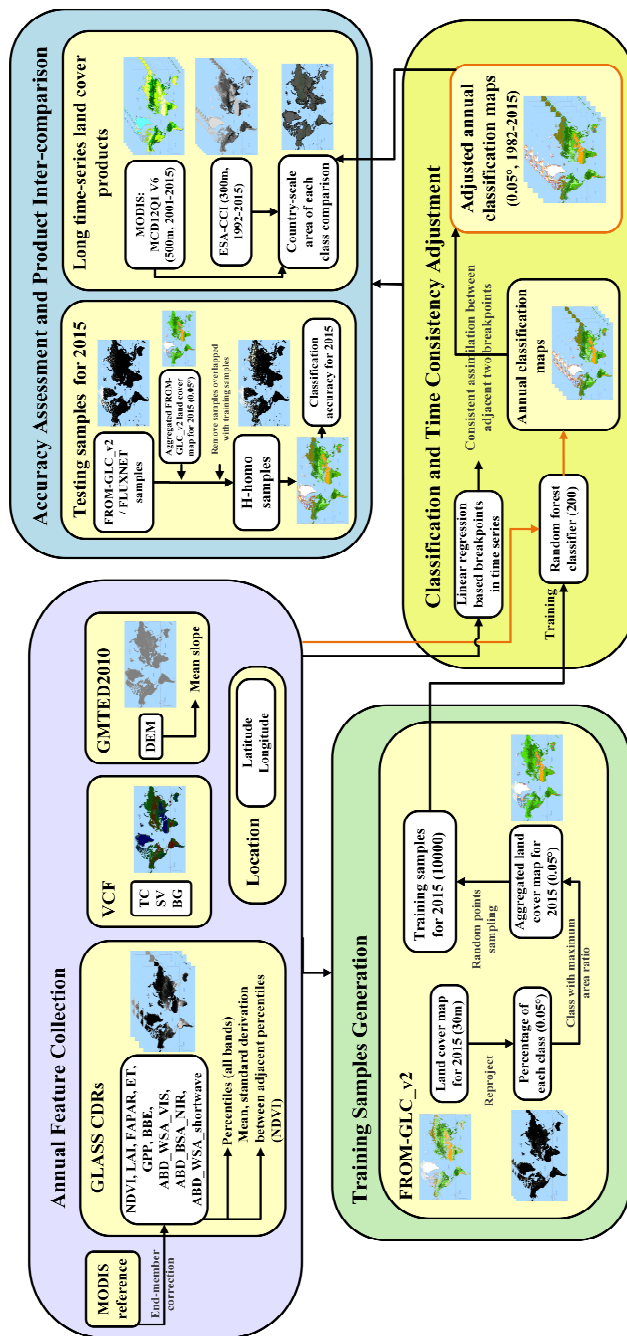


Figure 1: The framework for building GLASS-GLC (annual dynamics of global land cover) CDRs (Climate Data Records).



905 **Table 1: Classification system, with 7 Level 1 classes and 21 Level 2 classes.**

Level 1 class		Level 2 class				
Cropland	Rice fields	Greenhouse farming	Other croplands	Orchards	Bare farmlands	
Forest	Broadleaf forests, leaf-on	Broadleaf forests, leaf-off	Needleleaf forests, leaf-on	Needleleaf forests, leaf-off	Mixed forests, leaf-on	Mixed forests, leaf-off
Grassland	Pastures	Natural grasslands	Grasslands, leaf-off			
Shrubland	Shrublands, leaf-on	Shrublands, leaf-off				
Tundra	Herbaceous tundra	Shrub and brush tundra				
Barren land						
Snow/ice	Snow	Ice				

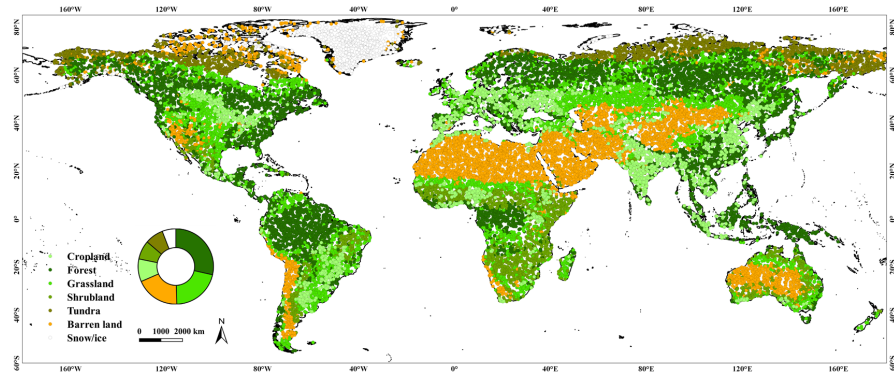


Figure 2: The geographical distribution of training samples, where different colors represent the different years.

910

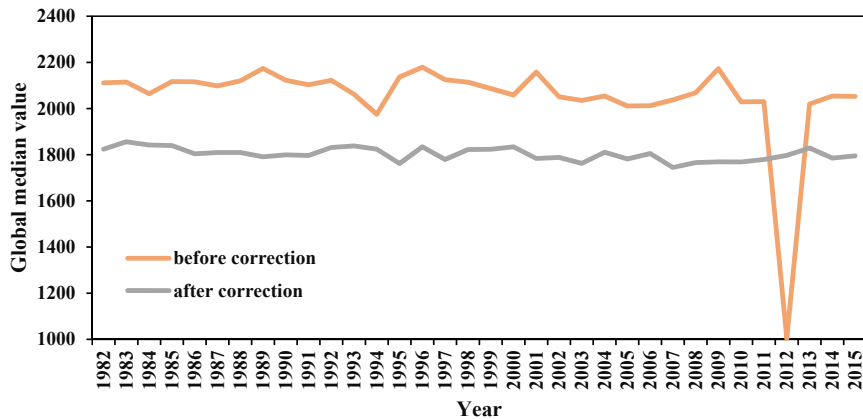
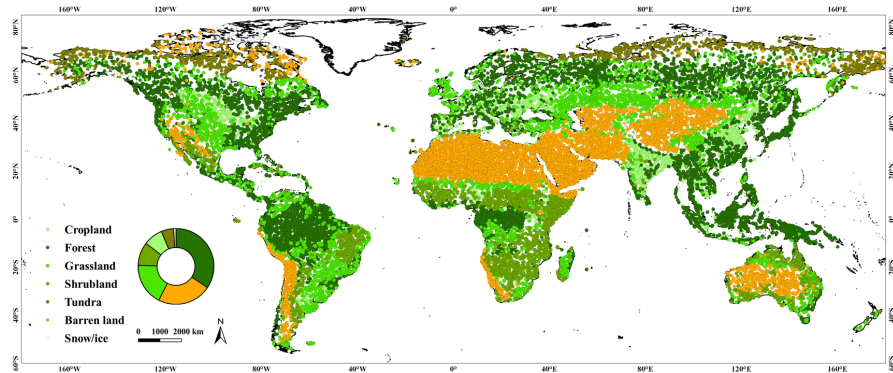


Figure 3: Global median value time series of GLASS ABD\_WSA\_VIS before and after the end-member correction with reference to MODIS.



915 **Table 2: The explanatory table of the constructed feature collection, with a total 81 features each year.**

Product	Band	Feature	Number of features
GLASS CDR, 0.05 °, 1982-2015	NDVI		
	LAI	Percentiles [0, 10, 25, 50, 75, 90, 100] of all 10 bands	63
	FAPAR		
	ET		
	GPP		
	BBE	Mean, standard derivation of NDVI between adjacent two percentiles of NDVI	12
	ABD_WSA_VIS		
	ABD_BSA_NIR		
	ABD_WSA_shortwave		
VCF, 0.05 °, 1982-2015	TC	TC	
	SV	SV	3
	BG	BG	
GMTED2010, 7.5 s, 2010	DEM	Mean slope in each 0.05 ° pixel	1
Location	Latitude, longitude	Center latitude, longitude of each 0.05 ° pixel	2
Total number of features			81



**Figure 4:** The geographical distribution of different types of huge homogeneous test samples (H-homo sample), where the different

920 colors represent the source of the sample units, either FROM-GLC\_v2 or FLUXNET.

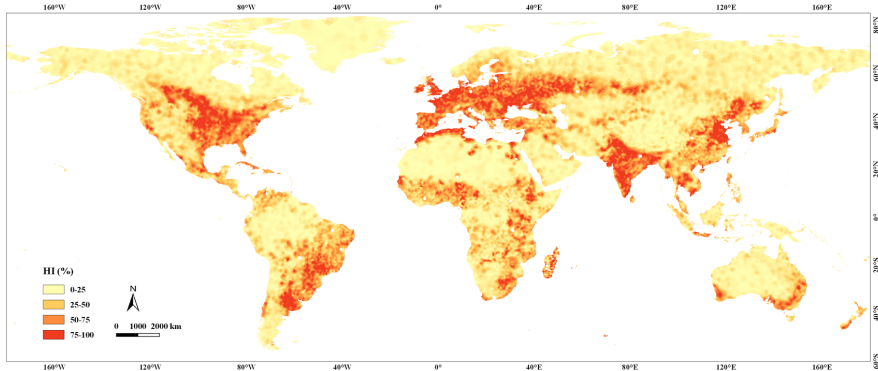


**Figure 5:** The geographical distribution of the spatial interpolation results of human impact where the darker color indicates a value closer to 100 and a higher human impact.

925

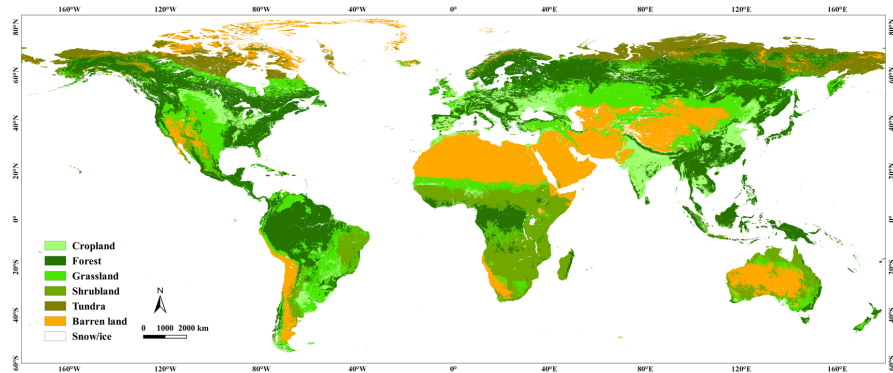


Figure 6: GLASS-GLC (annual dynamics of global land cover) CDRs (Climate Data Records) result in 2015.



**Table 3: Classification accuracy in 2015 based on FROM-GLC\_v2 test samples. (Overall accuracy = 86.51 %, UA = User's Accuracy**

930 **and PA = Producer's Accuracy)**

Class	Cropland	Forest	Grassland	Shrubland	Tundra	Barren land	Snow/ice	Total	UA
Cropland	<b>1390</b>	166	221	101	0	12	0	1890	73.54 %
Forest	115	<b>7427</b>	279	145	18	0	3	7987	92.99 %
Grassland	199	431	<b>2820</b>	534	45	141	3	4173	67.58 %
Shrubland	47	65	185	<b>1986</b>	0	92	0	2375	83.62 %
Tundra	0	32	36	0	<b>1157</b>	24	2	1251	92.49 %
Barren land	17	5	91	27	48	<b>5336</b>	20	5544	96.25 %
Snow/ice	0	2	10	0	7	41	<b>179</b>	239	74.90 %
Total	1768	8128	3642	2793	1275	5646	207	<b>23459</b>	
PA	78.62 %	91.38 %	77.43 %	71.11 %	90.75 %	94.51 %	86.47 %		<b>86.51 %</b>



**Table 4: Classification accuracy in 2015 based on FLUXNET testing samples. (Overall accuracy = 82.10 %, UA = User's Accuracy**

935 **and PA = Producer's Accuracy)**

Class	Cropland	Forest	Grassland	Shrubland	Tundra	Barren land	Snow/ice	Total number	UA
Cropland	<b>63</b>	5	17	1	0	0	0	86	73.26 %
Forest	13	<b>243</b>	9	2	0	0	0	267	91.01 %
Grassland	8	21	<b>91</b>	2	0	2	0	124	73.39 %
Shrubland	7	3	0	<b>19</b>	0	0	0	29	65.52 %
Tundra	0	3	0	0	<b>14</b>	0	0	17	82.35 %
Barren land	0	1	0	0	0	<b>1</b>	0	2	50.00 %
Snow/ice	0	0	0	0	0	0	<b>0</b>	0	-
Total number	91	276	117	24	14	3	0	<b>525</b>	
PA	69.23 %	88.04 %	77.78 %	79.17 %	100.00 %	33.33 %	-		<b>82.10 %</b>

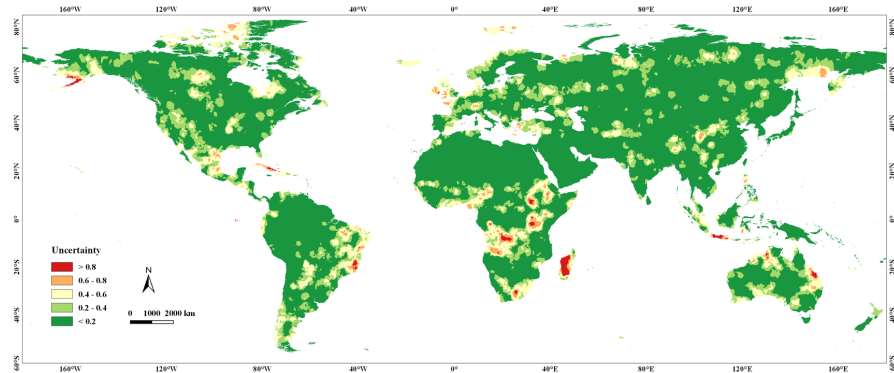


**Figure 7: The geographical distribution of uncertainty for GLASS-GLC (annual dynamics of global land cover) CDRs (Climate Data Records) in 2015, where regions in red represent higher uncertainty levels while those in green represent lower uncertainty levels.**

940

levels.

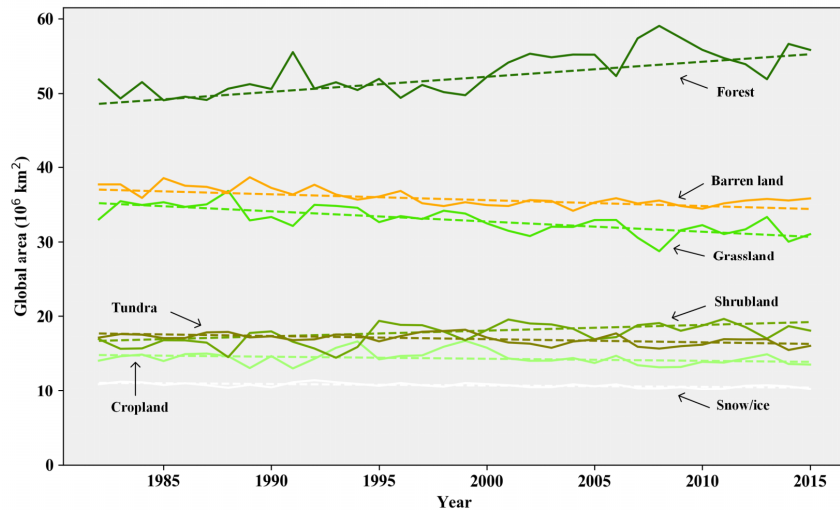
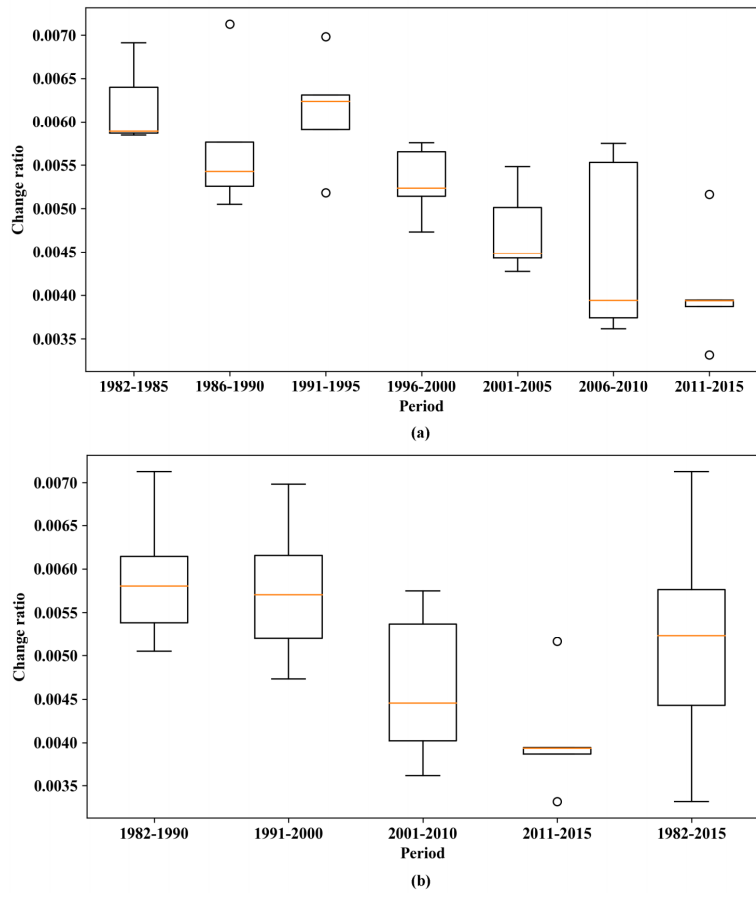
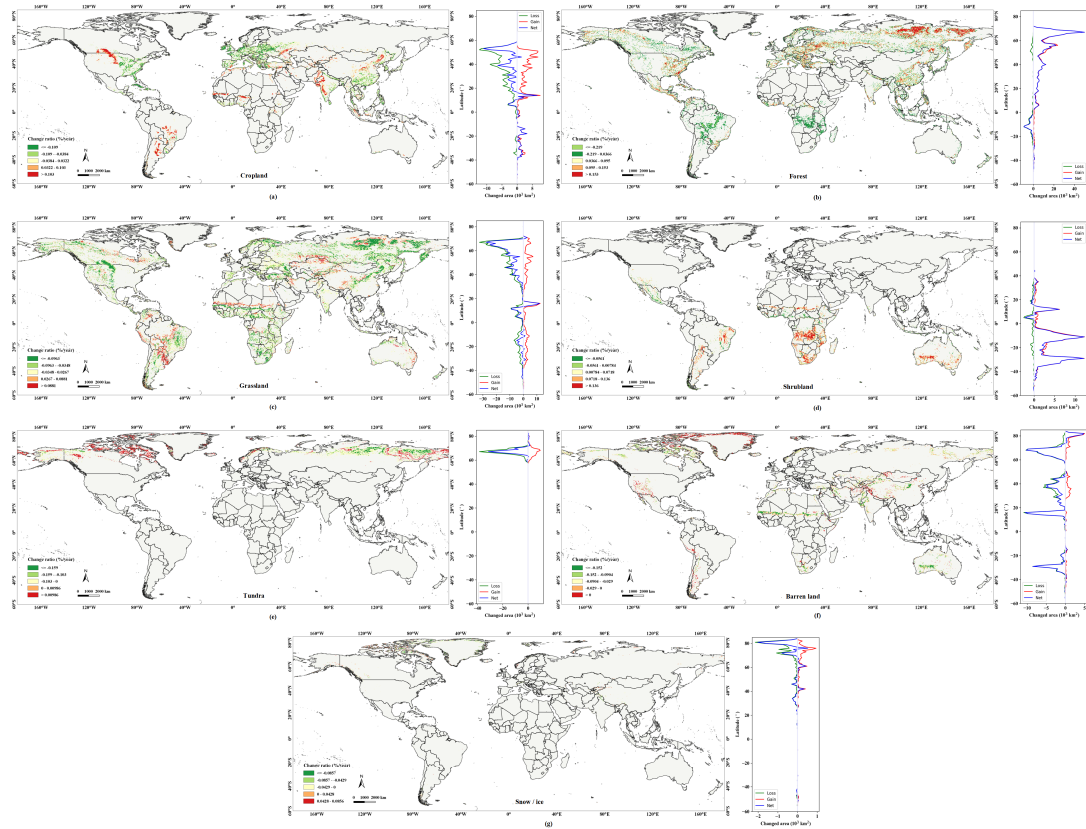


Figure 8: Area curves of global annual land cover change from 1982 to 2015.



945

**Figure 9: Comparison and distribution of ratios of annual global land cover change (LCC) to the global total terrestrial land cover (LC) area by different time periods and time intervals (a) 5-year interval, (b) 10-year interval.**



950      **Figure 10:** The geographical distribution of global regions with significant land cover change during 1982-2015, and the summarized results along latitudinal gradients for each class, (a) cropland, (b) forest, (c) grassland, (d) shrubland, (e) tundra, (f) barren land and (g) snow/ice.



**Table 5: Statistical results of change analysis for cropland (on the scale of continents). Annual change slope and its 95 % confidence**

955 **interval are given by Thei-sen estimator, p-value and trend information from a Mann-Kendall test. Gain and Loss areas are summarized results relating to the whole time series.**

Continent	Slope ( $10^3$ km $^2$ /year)	Lower ( $10^3$ km $^2$ /year)	Upper ( $10^3$ km $^2$ /year)	p	Trend	Gain ( $10^3$ km $^2$ )	Loss ( $10^3$ km $^2$ )
Africa	5.3	1.5	10.0	0.0099	increasing	23	-6
Asia	-1.7	-9.2	7.1	0.6999	no trend	67	-70
Europe	-30.4	-43.6	-17.9	0.0005	decreasing	12	-99
North America	-4.9	-10.9	2.8	0.1635	no trend	37	-54
South America	9.1	2.1	19.3	0.0108	increasing	35	-4
Oceania	-0.5	-1.8	0.6	0.3580	no trend	1	-1
Global	-27.5	-54.7	3.1	0.0968	no trend	175	-238



**Table 6: Statistical results of change analysis for forest (on the scale of continents) . Annual change slope and its 95 % confidence**

960 interval are given by Thei-sen estimator, p-value and trend information from a Mann-Kendall test. Gain and Loss areas are summarized results relating to the whole time series.

Continent	Slope ( $10^3$ km $^2$ /year)	Lower ( $10^3$ km $^2$ /year)	Upper ( $10^3$ km $^2$ /year)	p	Trend	Gain ( $10^3$ km $^2$ )	Loss ( $10^3$ km $^2$ )
Africa	-8.4	-18.6	2.6	0.1463	no trend	15	-29
Asia	128.6	86.8	165.0	0.0000	increasing	365	-12
Europe	53.1	34.9	67.4	0.0000	increasing	131	-1
North America	45.1	24.7	65.0	0.0000	increasing	132	-16
South America	-10.8	-19.6	-1.4	0.0242	decreasing	23	-49
Oceania	1.4	-0.1	2.6	0.0802	no trend	6	-1
Global	201.3	120.9	278.1	0.0000	increasing	680	-109



**Table 7: Statistical results of change analysis for grassland (on the scale of continents). Annual change slope and its 95 % confidence**

965 interval are given by Thei-sen estimator, p-value and trend information from a Mann-Kendall test. Gain and Loss areas are summarized results relating to the whole time series.

Continent	Slope ( $10^3$ km $^2$ /year)	Lower ( $10^3$ km $^2$ /year)	Upper ( $10^3$ km $^2$ /year)	p	Trend	Gain ( $10^3$ km $^2$ )	Loss ( $10^3$ km $^2$ )
Africa	-18.9	-36.4	3.0	0.0855	no trend	50	-108
Asia	-52.7	-67.1	-38.1	0.0000	decreasing	85	-315
Europe	-11.8	-21.7	-2.0	0.0207	decreasing	6	-59
North America	-39.6	-48.4	-26.9	0.0000	decreasing	25	-114
South America	-16.1	-29.0	-4.7	0.0070	decreasing	68	-54
Oceania	-4.6	-9.5	0.7	0.1029	no trend	9	-11
Global	-136.6	-172.9	-86.4	0.0000	decreasing	246	-663



**Table 8: Statistical results of change analysis for shrubland (on the scale of continents). Annual change slope and its 95 % confidence**

970 interval are given by Thei-sen estimator, p-value and trend information from a Mann-Kendall test. Gain and Loss areas are summarized results relating to the whole time series.

Continent	Slope ( $10^3$ km $^2$ /year)	Lower ( $10^3$ km $^2$ /year)	Upper ( $10^3$ km $^2$ /year)	p	Trend	Gain ( $10^3$ km $^2$ )	Loss ( $10^3$ km $^2$ )
Africa	47.4	16.1	74.8	0.0030	increasing	120	-11
Asia	-0.2	-1.4	1.0	0.8125	no trend	1	-1
Europe	0.0	0.0	0.0	0.7561	no trend	0	0
North America	0.5	-3.0	5.0	0.8356	no trend	8	-7
South America	17.8	-0.5	34.7	0.0618	no trend	38	-6
Oceania	19.9	3.9	36.2	0.0150	increasing	38	-2
Global	75.6	26.1	125.3	0.0017	increasing	207	-28



**Table 9: Statistical results of change analysis for tundra (on the scale of continents) . Annual change slope and its 95 % confidence**

975 **interval are given by Thei-sen estimator, p-value and trend information from a Mann-Kendall test. Gain and Loss areas are summarized results relating to the whole time series.**

Continent	Slope ( $10^3$ km $^2$ /year)	Lower ( $10^3$ km $^2$ /year)	Upper ( $10^3$ km $^2$ /year)	p	Trend	Gain ( $10^3$ km $^2$ )	Loss ( $10^3$ km $^2$ )
Africa	0.0	0.0	0.0	1.0000	no trend	0	0
Asia	-46.7	-66.6	-25.3	0.0002	decreasing	24	-132
Europe	-4.1	-6.8	-2.0	0.0015	decreasing	3	-12
North America	11.4	0.6	21.5	0.0408	increasing	42	-22
South America	0.0	0.0	0.0	1.0000	no trend	0	0
Oceania	0.0	0.0	0.0	1.0000	no trend	0	0
Global	-42.0	-63.7	-20.9	0.0019	decreasing	71	-167



**Table 10: Statistical results of change analysis for barren land (on the scale of continents) . Annual change slope and its 95 %**

980 **confidence interval are given by Thei-sen estimator, p-value and trend information from a Mann-Kendall test. Gain and Loss areas  
are summarized results relating to the whole time series.**

Continent	Slope ( $10^3$ km $^2$ /year)	Lower ( $10^3$ km $^2$ /year)	Upper ( $10^3$ km $^2$ /year)	p	Trend	Gain ( $10^3$ km $^2$ )	Loss ( $10^3$ km $^2$ )
Africa	-26.1	-37.4	-17.7	0.0000	decreasing	2	-43
Asia	-28.3	-40.6	-18.1	0.0000	decreasing	12	-82
Europe	-2.8	-3.5	-1.8	0.0000	decreasing	0	-6
North America	-8.8	-21.3	-1.0	0.0353	decreasing	26	-49
South America	1.6	-2.3	5.3	0.3737	no trend	4	-5
Oceania	-16.8	-32.2	4.0	0.1161	no trend	0	-25
Global	-78.5	-116.4	-48.8	0.0001	decreasing	48	-213



**Table 11: Statistical results of change analysis for snow/ice (on the scale of continents). Annual change slope and its 95 % confidence**

985 interval are given by Thei-sen estimator, p-value and trend information from a Mann-Kendall test. Gain and Loss areas are summarized results relating to the whole time series.

Continent	Slope ( $10^3$ km $^2$ /year)	Lower ( $10^3$ km $^2$ /year)	Upper ( $10^3$ km $^2$ /year)	p	Trend	Gain ( $10^3$ km $^2$ )	Loss ( $10^3$ km $^2$ )
Africa	0.0	0.0	0.0	0.1342	no trend	0	0
Asia	-2.4	-4.6	-0.4	0.0117	decreasing	2	-2
Europe	-0.8	-1.2	-0.2	0.0091	decreasing	1	-1
North America	-12.6	-20.6	-6.3	0.0015	decreasing	4	-11
South America	-0.2	-0.3	-0.2	0.0000	decreasing	0	0
Oceania	0.0	-0.1	0.0	0.0856	no trend	0	0
Global	-19.2	-27.6	-9.1	0.0003	decreasing	8	-16

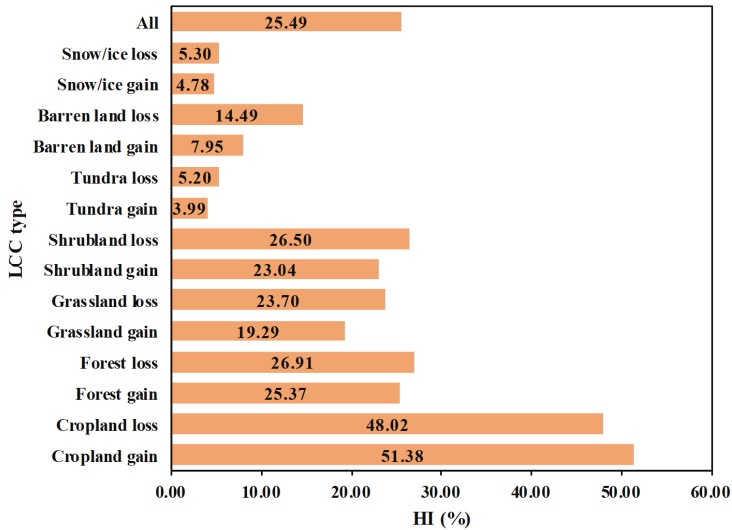


990 **Figure 11: Land cover conversions with significant land cover change (LCC) between 1982 and 2015.** The inner pie in (a) shows the percentages of different gross gain for each land cover, and the outer ring indicates which land cover the gross gain came from. The inner pie in (b) shows the percentage of different gross loss for each land cover, and the outer ring in indicates which land cover the gross loss went to.



995 **Table 12: Area ratio (%) of land cover conversions from 1982 to 2015, where the red color denotes a higher ratio, and the blue color represents a lower ratio.**

		2015						
Class		Cropland	Forest	Grassland	Shrubland	Tundra	Barren land	Snow/ice
1982	Cropland	-	9.6	2.22	0.37	0	0.09	0
	Forest	0.9	-	6.26	3.24	0.19	0.01	0.01
	Grassland	9.22	24.27	-	7.73	0.6	1.6	0.06
	Shrubland	0.45	1.7	1.62	-	0	0.66	0
	Tundra	0	8.48	3.82	0	-	0.79	0.04
	Barren land	3.07	0.07	5.75	2.23	2.93	-	0.29
	Snow/ice	0	0.05	0.13	0	0.13	1.43	-



1000    **Figure 12:** The mean human impact (HI) of regions with significant land cover change (on the scale of LCC).

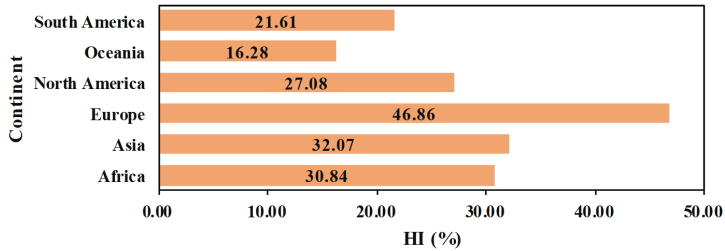
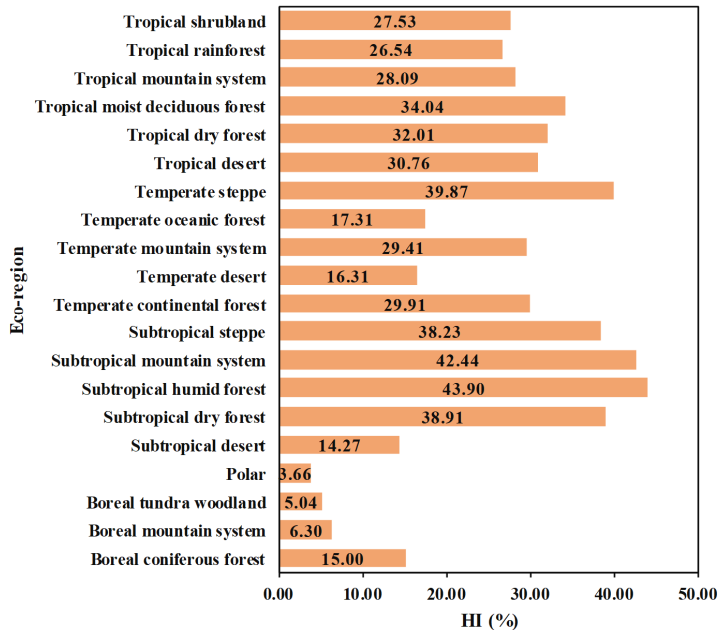


Figure 13: The mean human impact (HI) of regions with significant land cover change (on the scale of continents).



1005

Figure 14: The mean human impact (HI) of regions with significant land cover change (on the scale of eco-regions).

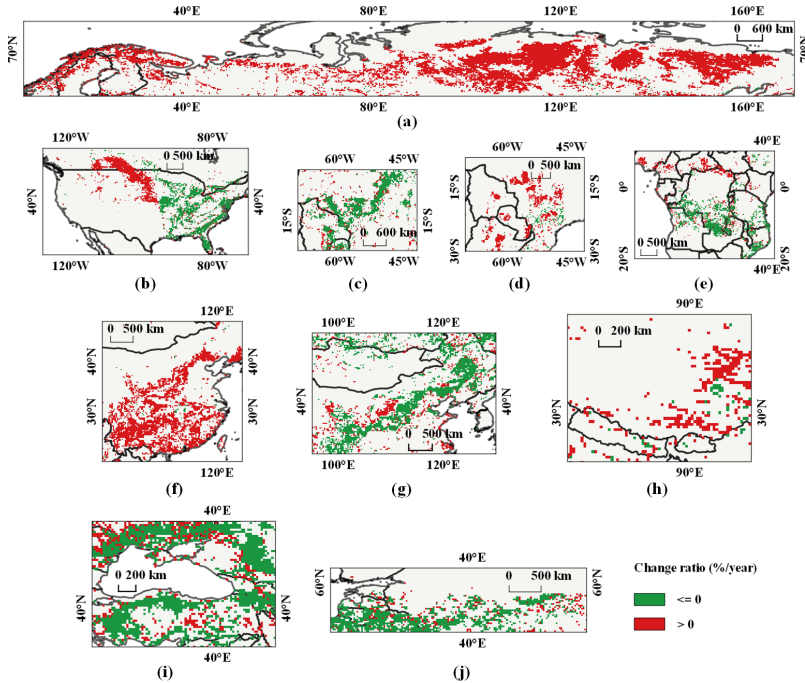
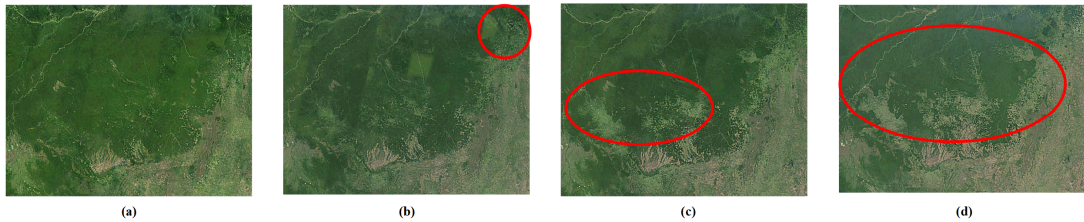


Figure 15: Visualization of local hotspots of land cover change, (a) north Eurasia, forest, (b) Great Plains of Central North America, 1010 cropland, (c) South America, forest, (d) South America, cropland, (e) Africa, forest, (f) China, forest, (g) Mongolia and Inner Mongolia of China, grassland, (h) Qinghai-Tibet Plateau, grassland, (i) central Asia, grassland, (j) the former Soviet Union in Eastern Europe, cropland.



1015 **Figure 16:** Example visualization for the cropland expansion and deforestation phenomenon in the southeastern part of the Amazon rainforest from Google Earth images in (a) 1984, (b) 1994, (c) 2000, (d) 2015, where the phenomenon is significant in area within red circles.